TG 1176
DECEMBER 1971
Copy No. 56

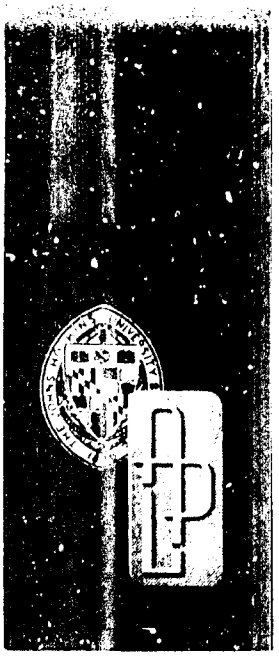

Technical Memorandum

SEAWATER BATTERY EXPERIMENTS

by J. P. WAGNER

THE JOHNS HOPKINS UNIVERSITY • APPLIED PHYSICS LABORATORY

75

UNCLASSIFIED

Security Classification

DOCUMENT CONTROL DATA - R & D

Security classification of title, body of abstract and indexing annotation must be entered when the overall report is classified)

1. ORIGINATING ACTIVITY (Corporate author)	2a. REPORT SECURITY CLASSIFICATION
The Johns Hopkins University, Applied Physics Lab. 8621 Georgia Ave. Silver Spring, Md. 20910	Unclassified 2b. GROUP

3. REPORT TITLE

Seawater Battery Experiments

4. DESCRIPTIVE NOTES (Type of report and inclusive dates)

Technical Memorandum

5. AUTHOR(S) (First name, middle initial, last name)

J. P. Wagner

6. REPORT DATE	7a. TOTAL NO. OF PAGES	7b. NO. OF REFS
December 1971	65	22

8a. CONTRACT OR GRANT NO.	9a. ORIGINATOR'S REPORT NUMBER(S)
N00017-72-C-4401 b. PROJECT NO.	TG 1176
c. d.	9b. OTHER REPORT NO(S) (Any other numbers that may be assigned this report)

10. DISTRIBUTION STATEMENT

Approved for public release; distribution unlimited.

11. SUPPLEMENTARY NOTES	12. SPONSORING MILITARY ACTIVITY
	Naval Ordnance Systems Command Department of the Navy

13. ABSTRACT

An experimental study pertaining to the development of a high energy density seawater battery is presented. In the initial phase of the study, cell orientation, cell geometry, electrode structure, and salinity effects were examined as to their effects on the current versus time characteristics and the electromotive force.

In the second phase, injection of nonreacting (nitrogen) and reacting (oxygen and chlorine) gases through the porous cathodes was investigated. Nitrogen had only a slight effect on increasing cell performance. With oxygen, noticeable improvements were obtained. With chlorine, the increases were dramatic.

Battery reaction mechanisms are discussed from an inductive viewpoint based on the Nernst equation and also from the theory of charge transport in ionic solutions.

The feasibility of employing the chlorine seawater battery for underwater applications is discussed.

DD FORM 1 NOV 68 1473

UNCLASSIFIED

Security Classification

14. KEY WORDS
Seawater batteries
High energy density batteries
Nonreacting gas injection
Reacting gas injection
Nernst equation
Charge transport theory
Underwater studies

TG 1176

DECEMBER 1971

Technical Memorandum

SEAWATER BATTERY EXPERIMENTS

by J. P. WAGNER

THE JOHNS HOPKINS UNIVERSITY • APPLIED PHYSICS LABORATORY
8621 Georgia Avenue, Silver Spring, Maryland 20910

Operating under Contract N00017-72-C-4401 with the Department of the Navy

THE JOHNS HOPKINS UNIVERSITY
APPLIED PHYSICS LABORATORY
SILVER SPRING MARYLAND

ABSTRACT

An experimental study pertaining to the development of a high energy density seawater battery is presented. The anode was a technical grade magnesium alloy, AZ31B-O (95.8 wt.% Mg), while the cathodes were sintered porous stainless steel with grain sizes of 165 micron, 35 micron, and 5 micron. In the initial phase of the study, cell orientation, cell geometry, electrode structure, and salinity effects were examined as to their effects on cell performance: current versus time characteristics and electromotive force (EMF). The highest current and power densities obtained were $J = 4.8$ A/ft^2 and $P_D = 2.06$ W/ft^2 for vertically oriented electrodes. The polarized cell EMF varied from only 0.4 volt to 0.5 volt for the 165-micron cathode over the wide range of parameters examined. A moderate dependence on cathode structure was observed; an EMF of 0.75 volt was measured for the 5-micron sample.

In the second phase, injection of non-reacting (nitrogen) and reacting (oxygen and chlorine) gases through the porous cathodes was investigated. Nitrogen had only a slight effect on increasing cell performance. With oxygen, a noticeable improvement was obtained; the mean current and power densities were $J = 18.6$ A/ft^2 and $P_D = 16.8$ W/ft^2. With chlorine, dramatic increases in J and P_D were obtained. J was as high as 177 A/ft^2 while P_D was 257 W/ft^2. The maximum projected power density based on the mean interelectrode spacing of 0.098 in and assumed (conservative) thicknesses of 1/32 in for the anode and cathode was 19.2 kW/ft^3. For both oxygen and chlorine, the cell EMF following injection also increased; it varied from 0.8 volt to 1.50 volts. No increases were obtained with nitrogen.

Battery reaction mechanisms are discussed from an inductive viewpoint based on the Nernst equation and also from the theory of charge transport in ionic solutions.

The feasibility of employing the chlorine seawater battery for underwater applications is discussed.

THE JOHNS HOPKINS UNIVERSITY
APPLIED PHYSICS LABORATORY
SILVER SPRING, MARYLAND

CONTENTS

ILLUSTRATIONS

ILLUSTRATIONS (cont'd)

ILLUSTRATIONS (cont'd)

LIST OF SYMBOLS

a	activity coefficient
A_a	anode area, L^2
A_c	cross-sectional area of cathode, L^2
A_{eff}	effective cross-sectional area, L^2
C	total ionic concentration, $C = C_+ + C_-$, moles/L^3
C^*	a molal type concentration, g/L^3
d	diameter, L
d_a	anode diameter, L
d_c	cathode diameter, L
D	diffusion coefficient, $D = \frac{D_+ + D_-}{2}$, L^2/t
D'	diffusion coefficient, $D' = \frac{D_+ - D_-}{2}$, L^2/t
E	reversible cell voltage, volts
E_o	standard half-cell voltage, V
E°	difference in standard half-cell voltages, V
F	Faraday constant, 96,500 C/eq
FC^o	total concentration of charge, C/L^3
h	charge transfer coefficient, cm/sec
I	current, mA
I_{ss}	steady-state or polarized cell current, mA

$I_{0.886}$ or $I_{1.672}$	current for a given anode diameter (in), mA
J	current density, A/L^2
K	conductivity, $R^{-1}L^{-1}$
K_{sp}	solubility product constant, dimensionless
K_D	Darcy permeability, L^2
ℓ	interelectrode spacing, L
L	electrode thickness, L
$\dot{m}$	mass flow rate, M/t
$\dot{M}_a$	rate of dissolution of anode, M/t
$\dot{M}_c$	difference between rate of formation and removal of H_2 at the cathode, M/t
Nu	Nusselt number, dimensionless
P_i	i-th product
P	porosity, dimensionless
P_D	power density, W/L^2
P_{DV}	power density per working volume, W/L^3
Δp	imposed pressure drop, F/L^2
q	charge density, $q = F(C_+ - C_-)$, C/L^3
r_i	i-th reactant
R	gas constant
t	time
T	Kelvin or absolute temperature, 273 + °C

u	ionic mobility, $L^2/V\text{-}t$
$\vec{v}$	vector flow velocity, L/t
v	cross-sectional velocity, L/t
v_o	superficial velocity, L/t
V_p	pore volume, L^3
V_t	total volume (solids plus voids), L^3
X_i	weight fraction, dimensionless
η_+	transference number for a positive ion, dimensionless
τ	relaxation time, $\tau = \varepsilon\varepsilon_o/K,t$
λ	film thickness, L
χ	hydrogen blockage factor, dimensionless
ρ	fluid density, M/L^3
μ	fluid viscosity, M/L-t

THE JOHNS HOPKINS UNIVERSITY
APPLIED PHYSICS LABORATORY
SILVER SPRING, MARYLAND

1. INTRODUCTION

The use of batteries as high energy, primary power sources for underwater applications, specifically propulsion, has been considered by a number of investigators at least as early as 1950 (Ref. 1). Batteries have several attractive features that are especially suitable to this type of environment: they are simple to operate (charge and recharge cycles), self-contained, portable, relatively independent of external conditions, have high conversion efficiencies ($\eta \simeq 85\%$), and generally have excellent storage properties. Although significant advances have been made in recent battery development programs, the principal drawback is their low energy densities, e.g., 30-150 W-hr/lb (at $\eta = 85\%$) (Ref. 2) versus values of around 1450 W-hr/lb (at $\eta = 25\%$) for conventional thermodynamic fuels (Ref. 3). In the lower region of the energy density range are batteries of moderate activity, e.g., the Ag-Zn battery and the seawater battery (Mg anode-inert cathode), while a battery made from elements or compounds at opposite extremes in the electrochemical activity series, such as the Li-Cl_2 battery, is illustrative of the upper region.

One aspect of interest in the Underwater Studies Program at APL is the development of a high energy density battery for underwater applications. The battery is subject to several rigid, yet arbitrary, constraints:

1. Generate 35 to 50 kW of continuous power for periods of up to 1 hour.
2. Operate within a cylindrical configuration, 21 inches x 7 feet, i.e., 16.8 ft^3.
3. Be reliable and have good storage properties.
4. Be cost effective.

The initial choice for study is the seawater battery because of low cost, high reliability, long life, and relative independence of operating depth and salinity (Ref. 4). Also, no protective case is required for electrolyte storage since the electrolyte is on-site seawater. Since a fivefold increase in the power output of present-day seawater batteries is needed to satisfy the above constraints (Ref. 5), more advanced electrochemical power sources are also being considered. They are a Mg anode-porous graphite cathode fuel battery using flowing liquid iodine at the cathode (Ref. 6), high temperature batteries having molten anodes and cathodes (Ref. 7), and a Li-Cl_2 battery similar to the Li-Sn battery in Ref. 8.

The present study examines the effects of a systematic variation of experimental parameters on the performance characteristics of a seawater battery. Although the results of this study demonstrate the feasibility of employing a seawater battery using gaseous chlorine injected through porous cathodes for practical high energy density applications, further study is required in a number of areas. Cell performance characteristics are needed for commercially available porous magnesium and lithium composites. Provisions for recycling the injected gas from cell to cell should be investigated, as well as other less toxic reacting gases or gas mixtures. Before scale-up of a small laboratory cell to a practical prototype much effort will be needed before the complex transport processes occurring within a seawater battery are adequately understood.

2. APPARATUS AND PROCEDURE

A schematic of the apparatus used in this study is given in Fig. 1. It consists of a cylindrical cell (d = 2-1/8 in, h = 3 in) of lucite and a measuring device to monitor current and voltage. Another cell made from a glass tube (d = 2 in, h = 4 in) and two rubber stoppers, one at each end of the tube, to hold the electrodes was used in the initial no-flow experiments. The lucite cell allowed one to measure accurately the interelectrode spacing and also prevented leakage of electrolyte during gaseous injection. The electrode holders were circular disks machined out of the inert plastics: Teflon, Nylon, and Lucite. The electrodes fit securely into the electrode holders for all non-flow tests. However, during the flow tests the cathodes were glued into the electrode holders in order to prevent gas leakage around the outer edge of the electrode and around the wire carrying the current to the measuring device.

Kintel microvolt ammeters Nos. 203R and 203A-R were used to measure current and voltage for all tests, except when the current exceeded 1 A, the upper limit of the ammeter. A standard Weston No. 430 ammeter sufficed for the higher amperages.

To ensure reproducibility and yet reuse the magnesium anode it was necessary to etch the magnesium before a run. A dilute solution of 3 N HCl was a satisfactory etching solution for the anode, as was a 2 N NaOH solution for the cathode for all runs in which a moderate reaction was observed. This occurred for values of P_D less than around P_D = 10 W/ft^2 and a solution pH $\simeq$ 7. A concentrated solution of HCl was used to dissolve a dark crud-like material that covered the anode for P_D values greater than 10 W/ft^2; the corresponding solution pH was 8.5. Because it was difficult to obtain reproducibility even after this foreign matter was removed, a new electrode was subsequently used whenever these conditions were observed. A white gel-like substance appeared on the cathode following the same vigorous reactions.

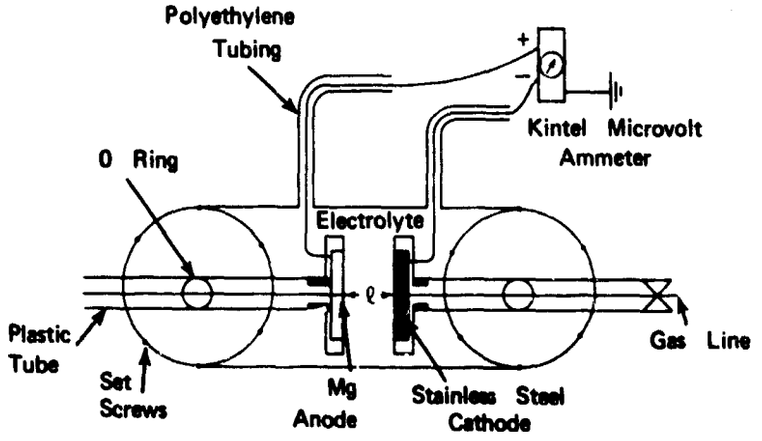

Fig. 1 SEAWATER TEST CELL

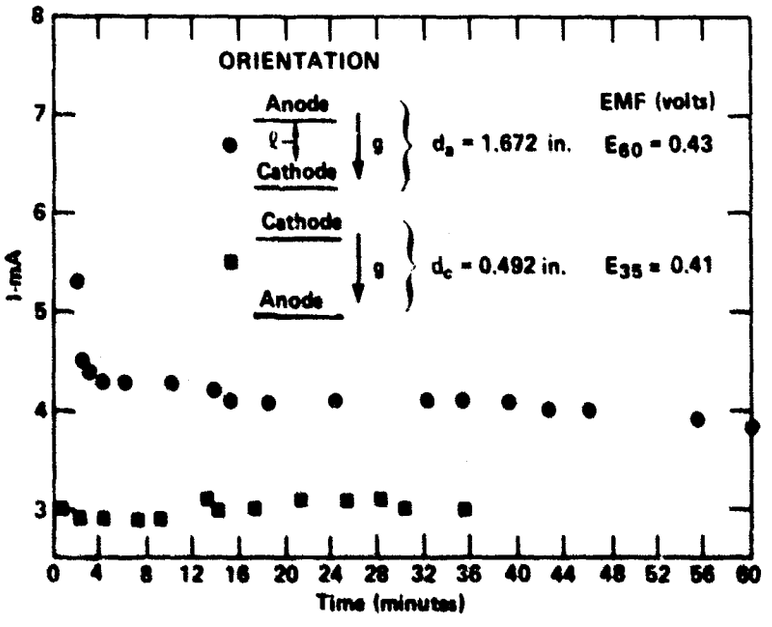

Fig. 2 CURRENT-TIME BEHAVIOR FOR TWO HORIZONTAL CELL ORIENTATIONS; ℓ = 0.63 INCH, A_c/A_a = 0.0665

Dilute 3 N HCl was used to dissolve this precipitate. For chlorine injection the stainless steel cathode was used only once since erosion occurred during testing. Following cleaning, both electrodes were rinsed with tap water and finally with copious quantities of distilled water. Current was then measured as a function of time.

3. EXPERIMENTAL RESULTS

CELL ORIENTATION AND GEOMETRICAL EFFECTS

Because of hydrogen evolution at the inert stainless steel cathode, the effects that free convection has on the current versus time characteristics were examined for three cell orientations: electrodes oriented horizontally (cathode lower and cathode upper), and electrodes aligned with gravity. In the paragraphs below a comparison is made between the performance characteristics for horizontal electrodes.

In Fig. 2 it is seen that an orientation having the cathode in the lower position leads to an increase in the current of about 33% (ℓ = 0.63 in). For the smallest mean interelectrode spacing tested, 0.098 in, the results in Fig. 3 show that for the first 24 minutes the mean current increases with increasing A_c/A_a. In Fig. 4, after the initial transient decay period of about 8 minutes, it appears that the current for the A_c/A_a = 0.0865 curve will be greater than that for A_c/A_a = 11.6. Although the results shown in Figs. 3 and 4 do not demonstrate which orientation is best, additional data shown in Fig. 14 again favor the cathode in the lower position. Another interesting observation of the data in Figs. 3 and 4 is that the current never approaches a steady-state value but fluctuates between an ill-defined upper and lower limit over short time intervals. Visual observation indicated that this effect was due to hydrogen gas evolution in the form of a large bubble for each discrete increase in the current.

Additional results for interelectrode spacings of ℓ = 0.315 in and 0.63 in presented in Figs. 5 and 6, respectively, show an orderly approach to a steady-state current with increasing time. Note also that the current extrapolated to t = 0 on semilog plots (not shown) shows an orderly increase with A_c/A_a. Another important observation is that the EMF for t > 25 min only varied between 0.41 to 0.50 volt for A_c/A_a = 1.00, 3.25, 11.6 and 16.5. Because of this observation the EMF was

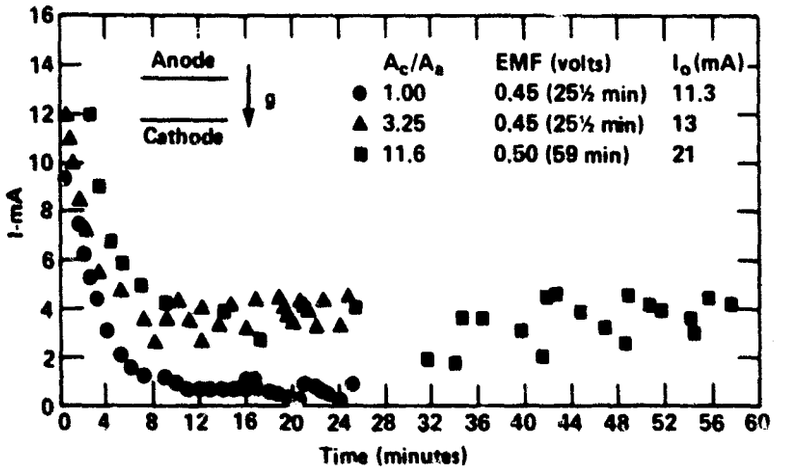

Fig. 3 CURRENT-TIME BEHAVIOR FOR DIFFERENT CATHODE TO ANODE AREA RATIOS, A_c/A_a, AT A HORIZONTAL ORIENTATION; ℓ = 0.098 INCH, d_a = 0.492 INCH

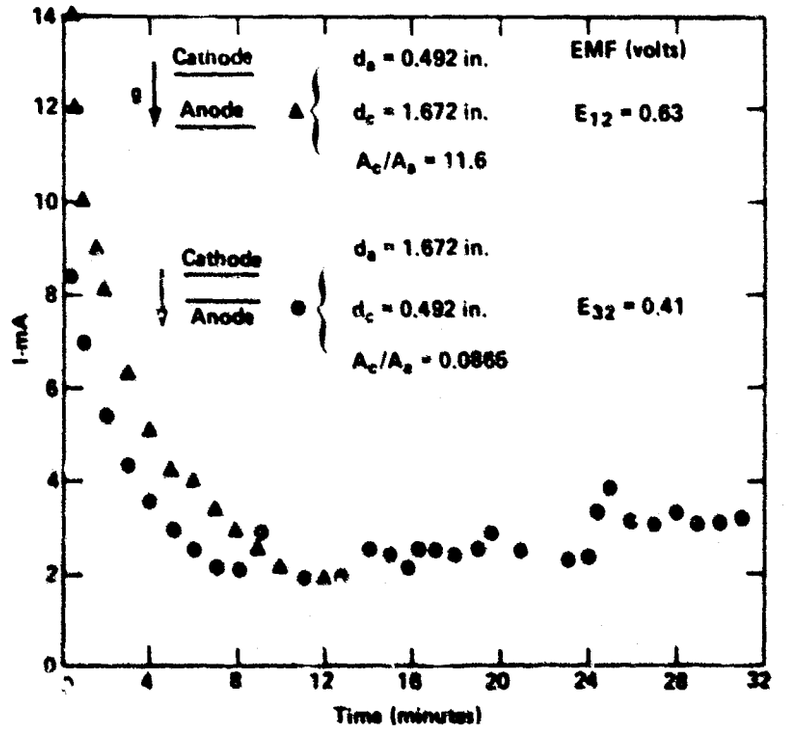

Fig. 4 CURRENT-TIME BEHAVIOR FOR TWO DIFFERENT AREA RATIOS, A_c/A_a, AT A HORIZONTAL ORIENTATION; ℓ = 0.098 INCH

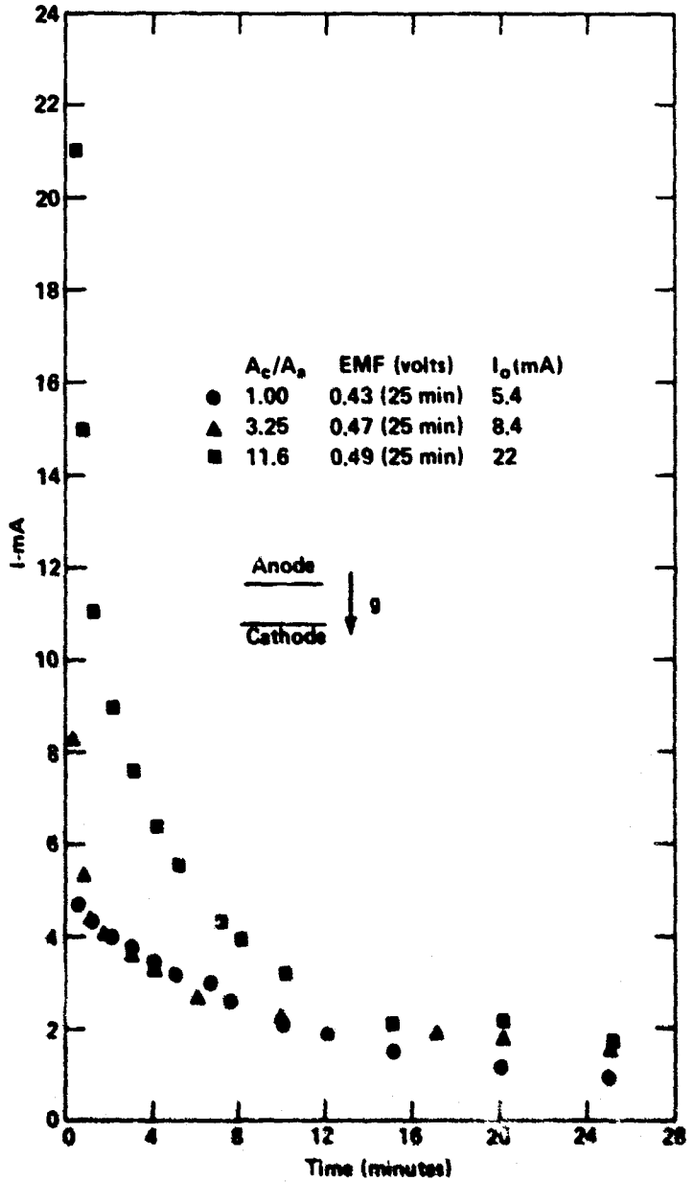

Fig. 5 CURRENT-TIME BEHAVIOR FOR DIFFERENT CATHODE TO ANODE AREA RATIOS, A_c/A_a, AT A HORIZONTAL ORIENTATION; ℓ = 0.315 INCH, d_g = 0.492 INCH

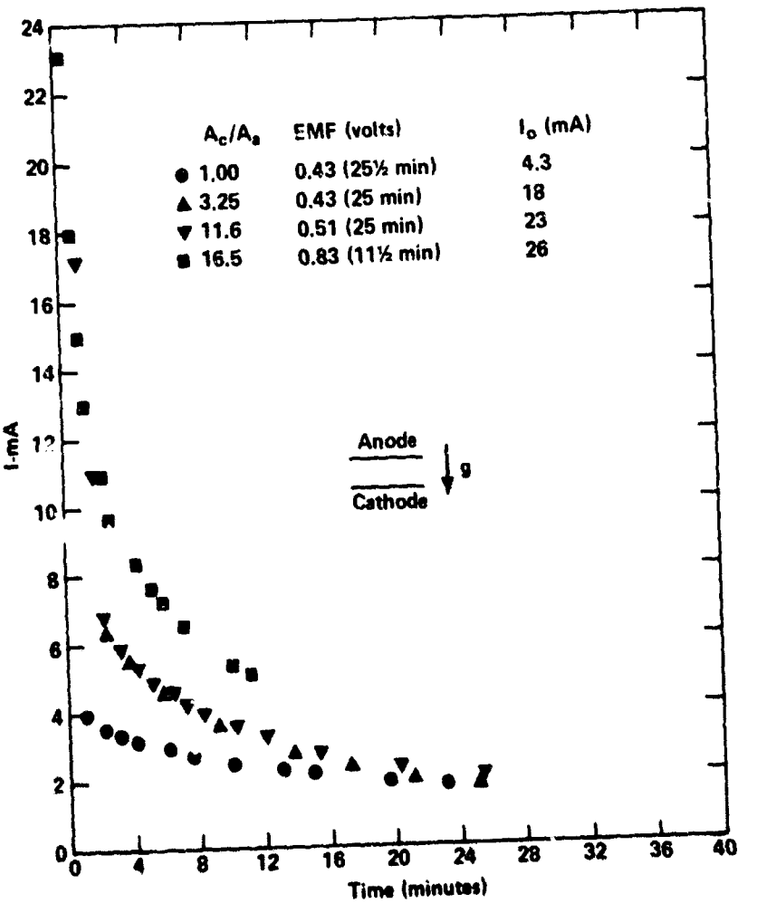

Fig. 6 CURRENT-TIME BEHAVIOR FOR DIFFERENT CATHODE TO ANODE AREA RATIOS, A_c/A_a, AT A HORIZONTAL ORIENTATION; ℓ = 0.63 INCH, d_a = 0.492 INCH

measured following the initial transient current decay. Preliminary tests showed a slight decrease of the cell voltage with time; however, once the current was measured (for times as short as $t \simeq 30$ sec) and then the cell voltage remeasured, a decrease in the EMF by around a factor of 2 was observed. Computation of the power output based on a polarized cell current and the corresponding EMF will, therefore, lead to a conservative value for the effective power output of a cell.

The current-time behavior shown in Fig. 7 is illustrative of the data obtained for vertically oriented electrodes at an interelectrode spacing of 0.098 in and large values of A_c/A_a (here $A_c/A_a = 11.6$). The current fluctuates between a lower base level of about 4 mA and an upper limit of 6 mA after the decay of the transient current. Here the mean current is around 5 mA. This is a considerable improvement over the 2 to 3 mA obtained for the horizontally oriented electrodes of Figs. 3 and 4. An EMF of 0.42 volt at 64 minutes again lies within the EMF range obtained previously. Thus the cell's current density, power output, and power density are greater for vertically oriented electrodes than for horizontal orientations. Additional experimental evidence that supports this observation is given in Fig. 14. It is also clear that the steady-state power outputs of the cells are greatest for the smallest interelectrode spacing tested -- 0.098 in.

ANODE EFFECTS

In this section the effect of variation of anode area was examined for values of $A_c/A_a = 1.00$, 3.25, and 3.56. Here the intent is to determine whether or not the current and the power densities are radially uniform. Or, in other words, is one justified in using values of current density and power density obtained on small lab-type cells to make estimates of overall power outputs on much larger cells (a scaling-up problem), when the mechanisms of mass transport and hydrogen bubble formation and evolution are, at best, incompletely understood.

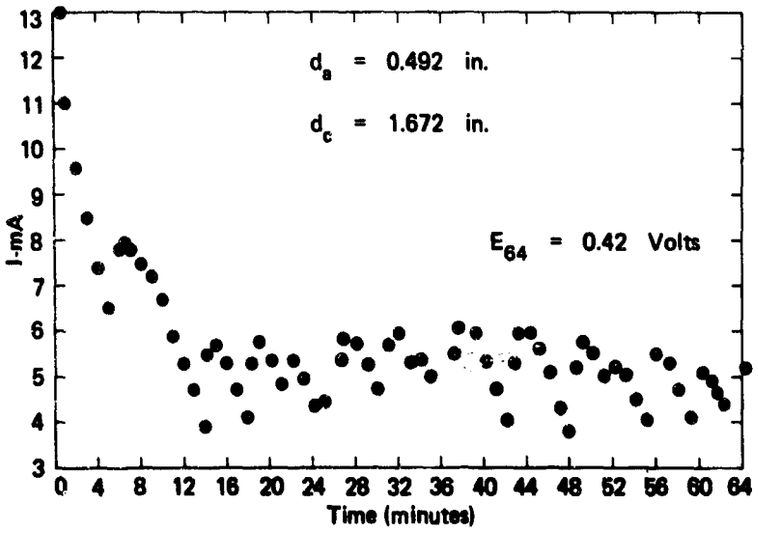

Fig. 7 EFFECT OF HYDROGEN EVOLUTION ON THE CURRENT-TIME CHARACTERISTICS FOR A VERTICALLY ORIENTED CELL AT A_c/A_a = 11.6, ℓ = 0.098 INCH

In Fig. 8 a comparison of the current-time characteristics is made for three different anode diameters: 0.492 in, 0.886 in, 1.672 in at $A_c/A_a = 1.00$ for horizontal orientation. In going from $d = 0.492$ in to 0.886 in the current following the initial transient decay increased by about tenfold, while the area only changed by a factor of 3.25. An increase in d from $d = 0.886$ to $d = 1.672$ did not lead to a corresponding uniform increase in I; actually the I's at $t = 12$ minutes are nearly equal. In Fig. 9 similar comparisons are made for a vertical cell orientation. A steady-state current of around 6.3 mA for the $d = 0.492$-in anode should correspond to a value of 20.5 mA at $d = 0.886$; this is reasonably close to the observed value of 18.5 at $d = 0.886$ in. In going to $d = 1.672$ in, one would expect a value of $I_{1.672} \simeq 3.56\ I_{0.886}$ or 61.9 mA. Values of 43 mA and 47 mA obtained on two separate runs fall far short of this projected value. Data points are only plotted up to $t = 14$ minutes since these runs were then subjected to gaseous injection and are plotted in Figs. 17 and 18. Further comparison in Fig. 10 for a $d = 0.492$-in anode at $A_c/A_a = 3.25$ with a $d = 0.886$-in anode at $A_c/A_a = 3.56$ is in close agreement since $I_{3.56}$ is expected to be roughly equal to $I_{3.56} = 3.25\ I_{3.25}$, where $I_{3.25} = 5.5$ mA. That is, the projected value of 17.9 mA compares favorably with the observed value of 21 mA. It is again interesting to note that the EMF's only vary from 0.40 volt to 0.45 volt for the two orientations and the range of geometries over time intervals from 16 minutes up to 37 minutes. From a design viewpoint, the results presented in Figs. 8 - 10, inclusive, indicate that a cell made up of a series of small electrodes would have higher current and power densities than one made up of a single electrode of equivalent area. Or, alternatively, that the current density does not appear to be radially uniform.

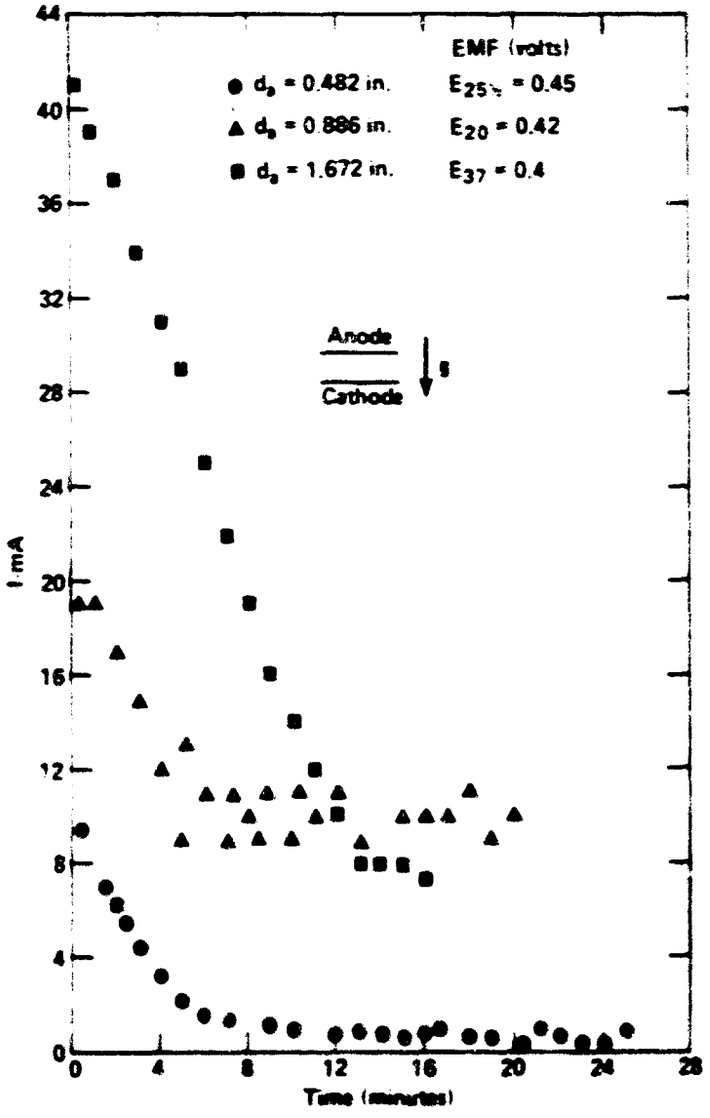

Fig. 8 CURRENT-TIME DEPENDENCE ON ANODE AREA FOR A HORIZONTAL CELL ORIENTATION AT A_c, A_a = 1.00, ℓ = 0.096 INCH

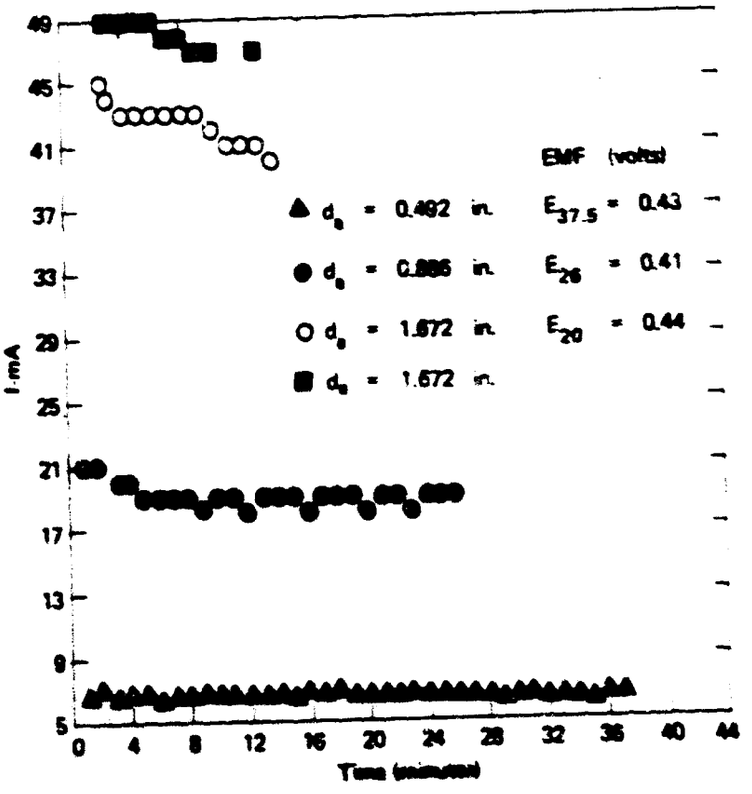

Fig. 9 CURRENT-TIME DEPENDENCE ON ANODE AREA FOR A VERTICAL CELL ORIENTATION; A_a/A_c = 1.89, ℓ = 0.088 INCH

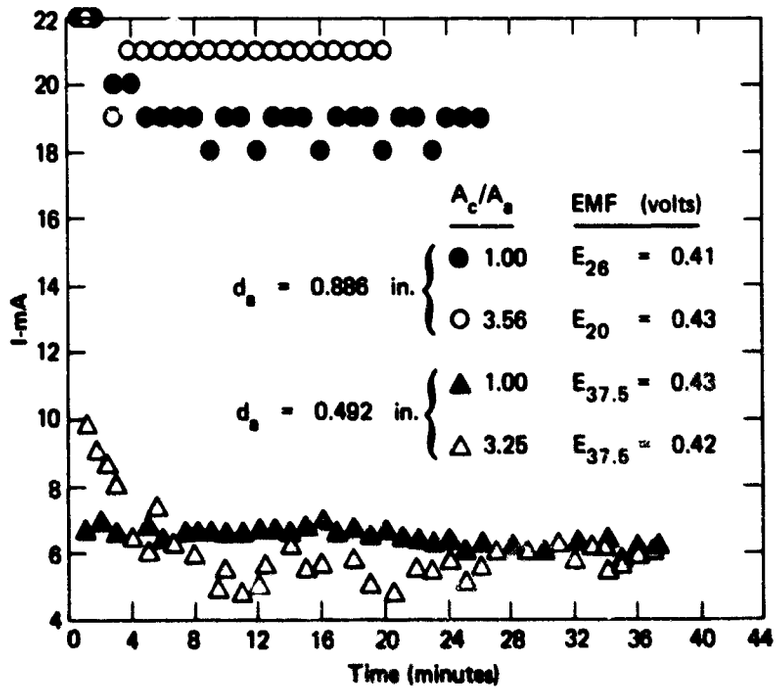

Fig. 10 COMPARISON OF CURRENT-TIME BEHAVIOR FOR TWO DIFFERENT ANODE AREAS AT SELECTED AREA RATIOS, A_c/A_a FOR A VERTICAL CELL ORIENTATION; ℓ = 0.098 INCH

CATHODE STRUCTURE

Porous stainless steel (316L) cathodes of three different grain sizes -- 165μ†, 35μ, and 5μ -- were examined as to their effect on the current-time behavior for two different cell orientations. In Fig. 11 one observes a somewhat similar overall behavior for all three grain sizes. Closer inspection reveals that the 165μ test has a higher lower trendline, lying between 2 mA and 2.8 mA, than either the 35μ or the 5μ, which form a baseline at about 0.5 mA. The upper data points for the 165μ and the 35μ runs are about equal, while the 35μ points are slightly lower. Even though the EMF for the 165μ run measured at t = 58 min is 16.7% and 33% lower than the EMF's at t = 31 min and t = 25 min for the 35μ and 5μ cathodes, respectively, these differences are not sufficient to increase the cell power output above that of the 165μ cell.

The data in Fig. 12 for 35% salinity clearly show that a 165μ cathode more effectively reduces cell polarization than the 35μ cathode. The 5μ cathode was not tested because it appeared that its pores were more prone to clogging by cathodic deposits than either the 35μ or the 165μ cathodes.

The porosities of the 165μ, 35μ, and 5μ samples are 60.5%, 46.5%, and 43%, respectively. From a structural viewpoint the 165μ cathode would again be preferred because it has the largest surface area (PA_C) perpendicular to the direction of charge transport.

SALINITY EFFECTS

Artificial seawater representing a typical analysis of seawater (Ref. 9) was prepared by dissolving properly ratioed quantities of NaCl, Na_2SO_4, $MgCl_2$, KCl, and $CaSO_4$ in a measured

†The cathodes in Figs. 2 - 10 and 13 - 20 were the 165μ grain size.

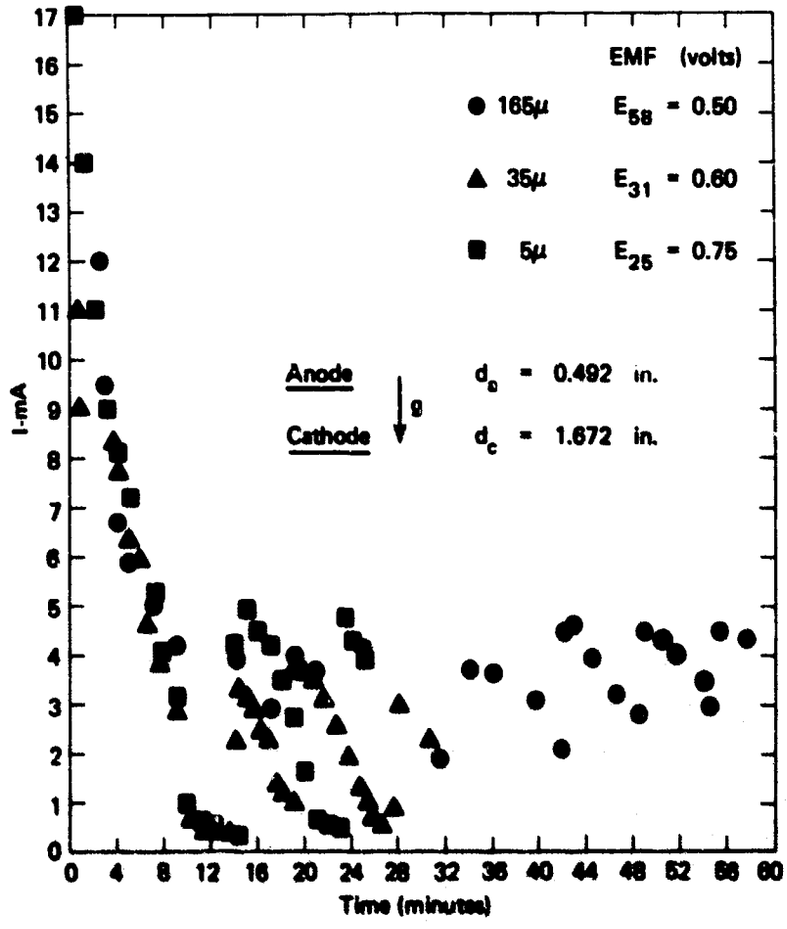

Fig. 11 CURRENT-TIME BEHAVIOR FOR THREE DIFFERENT CATHODE PORE SIZES AND A HORIZONTAL CELL ORIENTATION; ℓ = 0.098 INCH, A_c/A_a = 11.6

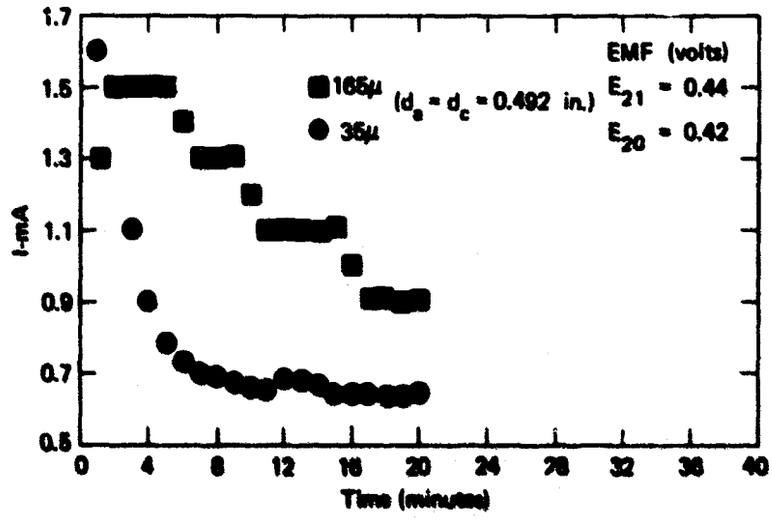

Fig. 12 CURRENT-TIME BEHAVIOR FOR TWO DIFFERENT CATHODE PORE SIZES AT 35% SALINITY AND VERTICAL CELL ORIENTATION; ℓ = 0.098 INCH, A_a/A_c = 1.00

volume of distilled water. Compounds containing Br^-, $BO_3^{\equiv}$, and $PO_4^{\equiv}$ were not added since these anions were present in concentrations not exceeding 67 ppm. The effects of salinity† on I versus t data are shown in Fig. 13 (see also Fig. 18 and page 23 for an explanation of the flagged symbols). Here C* is a molal type concentration, i.e., a given amount of salt was added to a graduated cylinder and distilled water was added to make the volume equal to 1ℓ. For the lower concentrations C may be used interchangeably with C*, since the final solution volume is essentially independent of small quantities of salt.

The data show a rather strong dependence of the current on salinity. For high salinities the current is not uniform with time. The non-uniform behavior is not identical to the type of behavior observed previously for the discrete hydrogen evolution in Figs. 3, 4, and 7. It appeared that chunks of reacted anode material (a dark crud-like substance) broke off the surface, thereby exposing a fresh surface that led to the increase in the current. The solution became cloudy and the pH changed from about 6.5 - 7.0 before the test to 9.5 after. A white precipitate also deposited on the stainless steel cathode. The dark crud appears to be a mixture of metallic hydroxides resulting from the primary and secondary cell reactions given in Ref. 10:

Primary reaction		E^o
Anode	$Mg \rightarrow Mg^{++} + 2e^-$	2.37
Cathode	$2H_2O + 2e^- \rightarrow 2OH^- + H_2$	-0.828
	$Mg + 2H_2O \rightarrow Mg(OH)_2\downarrow + H_2\uparrow$	1.542

† For the I versus t data given in Figs. 1 - 11 and 14 - 17, the salinity is 7 g/l. The salinity is defined as grams salt/kg solution x 100%.

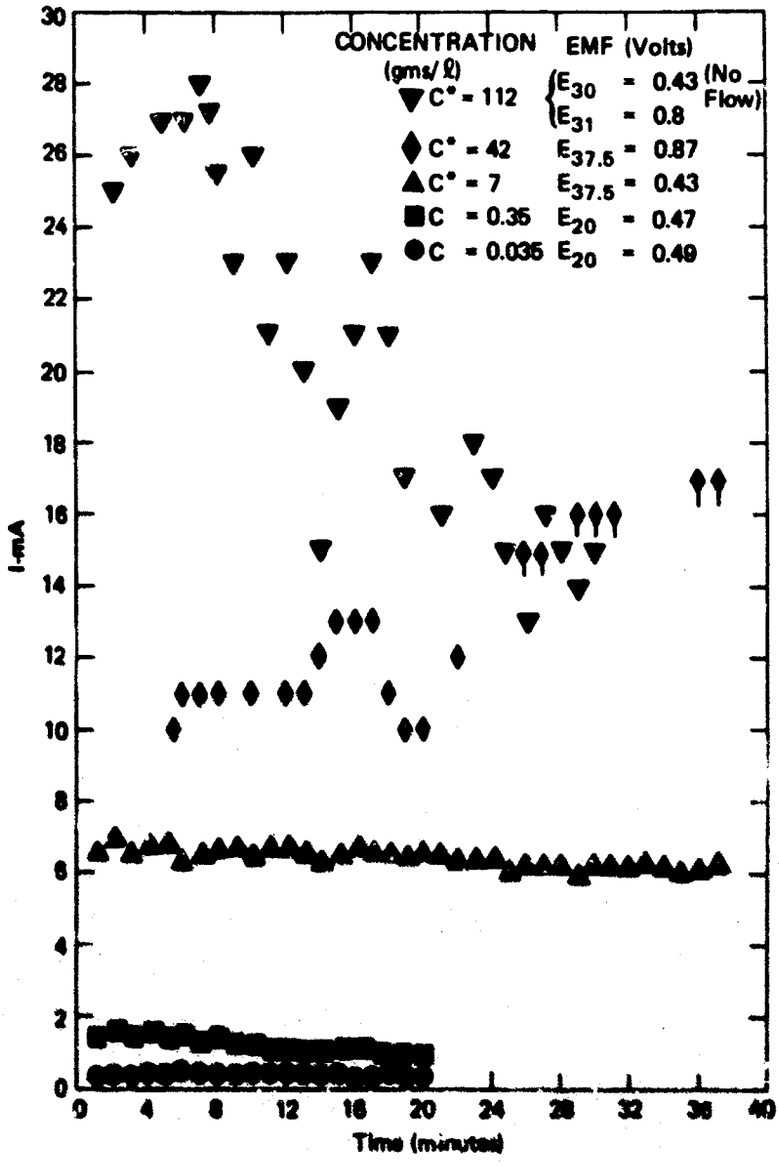

Fig. 13 EFFECT OF CONCENTRATION OF ELECTROLYTE ON THE CURRENT-TIME CHARACTERISTICS FOR A VERTICALLY ORIENTED CELL; ℓ = 0.008 INCH, A_c/A_a = 1.00

Secondary reaction

$$NaOH + MgCl_2 \rightarrow 2NaCl + Mg(OH)_2 \downarrow$$

obtained from

Anode $\quad 2Cl^- + Mg^{++} \rightleftharpoons MgCl_2$

Cathode $\quad OH^- + Na^+ \rightleftharpoons NaOH$

The white precipitate is probably a mixture of calcium and aluminum hydroxides.

Higher salinities than the $C^* = 112$ g/l were tested; however, the measured current dropped abruptly after a few minutes from the mA range to the μA range. Upon reducing the electrode distance to the point where the electrodes were touching, the current again returned to the mA range. In all cases the current was much less than that obtained for the $C^* = 112$ g/l test. It is possible that at extremely high salt concentrations a cell is set up between the wire leading to the measuring device and the anode which results in shorting out the main cell reaction. No effort was made to explore possible methods of circumventing this effect.

The strong dependence of cell reactivity on salinity is in contrast to the relative independence pointed out in Ref. 4. This apparent discrepancy is probably due to the use of a different type of a cathode (sintered porous stainless steel, type 316L) over a wider range of salinity. Chemical composition of the anode and the nature of its surface also enter into the problem. For example, pure magnesium will react in moist air (Refs. 11 and 12), whereas high salinity solutions are needed for appreciable reaction with the AZ31B-O magnesium alloy.

GASEOUS INJECTION EFFECTS

Nonreactive Gases -- Nitrogen

As previously observed, e.g., Figs. 3, 4, and 7, removal of H_2 gas from the electrode

surfaces via a free-convective process leads to a discrete increase in the current. In this second phase of the study, the effects of gaseous injection through the porous cathodes (a forced convective process) on the current-time behavior are examined for nonreactive and reactive gases. Here nonreactive means that the foreign gas cannot undergo a reaction with the seawater reaction scheme given on page 20 while the contrary holds for a reactive gas. A discussion of possible mechanisms whereby the two reactive gases can undergo chemical reaction is given in Section 6 on the seawater reaction mechanism.

In Fig. 14 a comparison is made between the effects of N_2 injection on the current-time characteristics for three cell orientations at $A_c/A_a = 1.00$. The solid vertical line drawn through the bottom of any given symbol means that gas flow was started immediately after that data point was recorded; the two solid vertical lines around 5 mA in Fig. 14 indicate that gas flow occurred at that corresponding time on the abscissa but that data points were not taken at these times. A single vertical line followed by ordinary symbols means that gas injection consisted of a pressure pulse generally lasting a few seconds (never more than around 10 sec); two or more flagged symbols mean that the injection was operated in a continuous mode over that time interval. An estimate of the amount of gas injected is given in the Appendix.

For the vertically oriented electrodes a slight increase in the current following injection from 4.9 mA to 5.3 mA is noted. For the horizontal case, in which the cathode was the lower electrode, a near doubling of the current took place from 2.3 mA to 4.5 mA after the first N_2 pulse and then from 2.1 mA to 3.5 mA after the second pulse. With the anode in the lower position the current increased slightly from 2.5 mA to 2.8 mA after pulsing. Since the EMF's were not affected by N_2 injection, that is, they are all once again around 0.4 - 0.5 volt, the vertically oriented cell has the highest power output. Also, the cell with the anode in the lower position (horizontal orientation) produced the lowest power output.

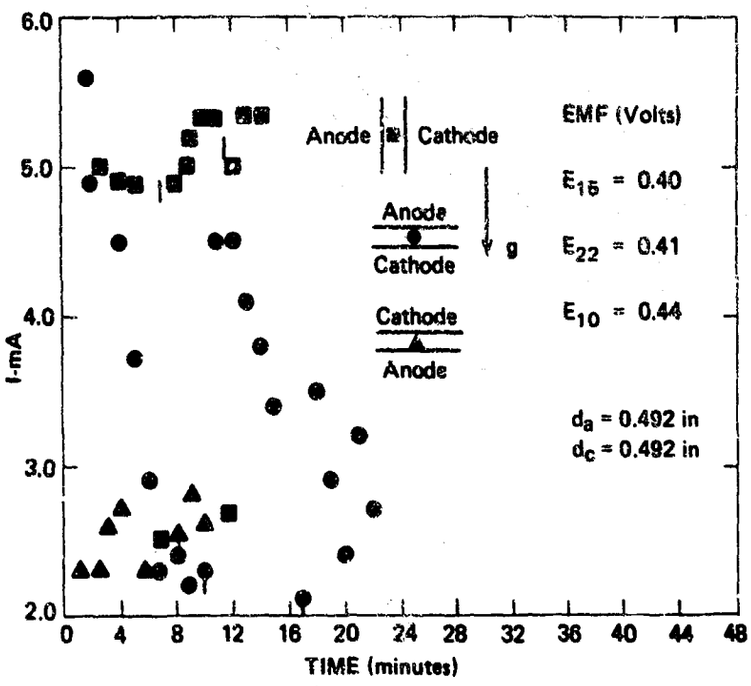

Fig. 14 COMPARISON OF THE EFFECTS OF NITROGEN INJECTION ON THE CURRENT-TIME CHARACTERISTICS FOR THREE CELL ORIENTATIONS; A_c/A_a = 1.00, ℓ = 0.098 INCH

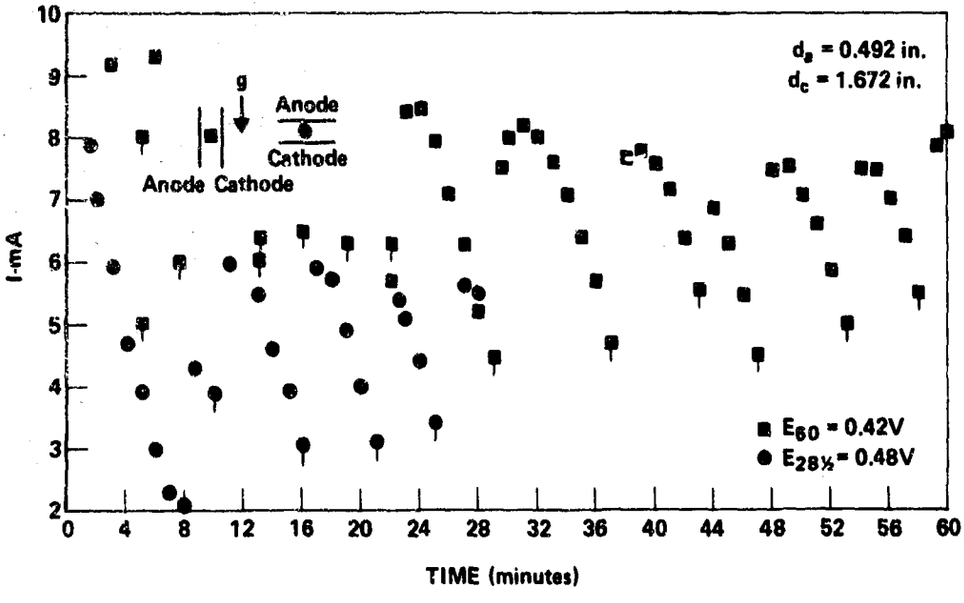

Fig. 15 EFFECT OF NITROGEN INJECTION ON THE CURRENT--TIME CHARACTERISTICS FOR TWO DIFFERENT CELL ORIENTATIONS; A_c/A_a = 11.6, ℓ = 0.098 INCH

In Fig. 15 the two best performing cells are compared for dissimilar electrode areas, A_c/A_a = 11.6. Once again, the current output is greater for the vertically oriented cell. Another important observation is that operating the cell in a continuous N_2 injection mode from t = 7½ min to t = 22 min did not lead to an increase in the current. Actually, any appreciable injection rates caused the current to fluctuate between upper and lower limits; note the data at t = 5, 13, and 22 min. Only after continuous injection was stopped and the cell operated in the pulse mode, e.g., at t = 22, 29, 37, and 43 min, etc., did the current increase from its baseline between 5 mA and 6 mA up to around 8 mA. Similar behavior was also observed for the horizontal orientation although the magnitudes differed.

In Fig. 16 the effect of N_2 injection on change in anode area at A_c/A_a = 1.00 is examined for horizontal orientation. The d = 1.672-in diameter anode run is the same as the shortened run in Fig. 8; the two remaining runs were repeats of the conditions tested in Fig. 8. The results shown in Fig. 16 in comparison with those of Fig. 8 show that the effect of forced convection gas injection on augmenting the current is greater than that of free or natural convection. This is easiest to see by comparing the 0.886-in and 1.672-in diameter runs in these two figures. For example, at t = 6 min (Fig. 16) the current went from 9 mA to 15 mA following injection, whereas the high-low for the corresponding case fluctuated between 9 mA and 11 mA for t = 5 min to t = 20 min. The current fell below 9 mA to a lower level of 6 mA following N_2 gas injection; however, this only occurred for a period of about 2 min where a second N_2 pulse increased its value to 13 mA.

For the d = 1.672-in anode (Fig. 16) the current at t = 16 min increased from about 7 mA to 17 mA following N_2 injection, whereas at t = 21 min the effect of natural convection resulted in an increase of I from 10 mA to 17 mA. An N_2 pulse later increased I from 17 mA to 21 mA. Also, at t = 29 min, an N_2 pulse raised the current from 10 mA to 19 mA.

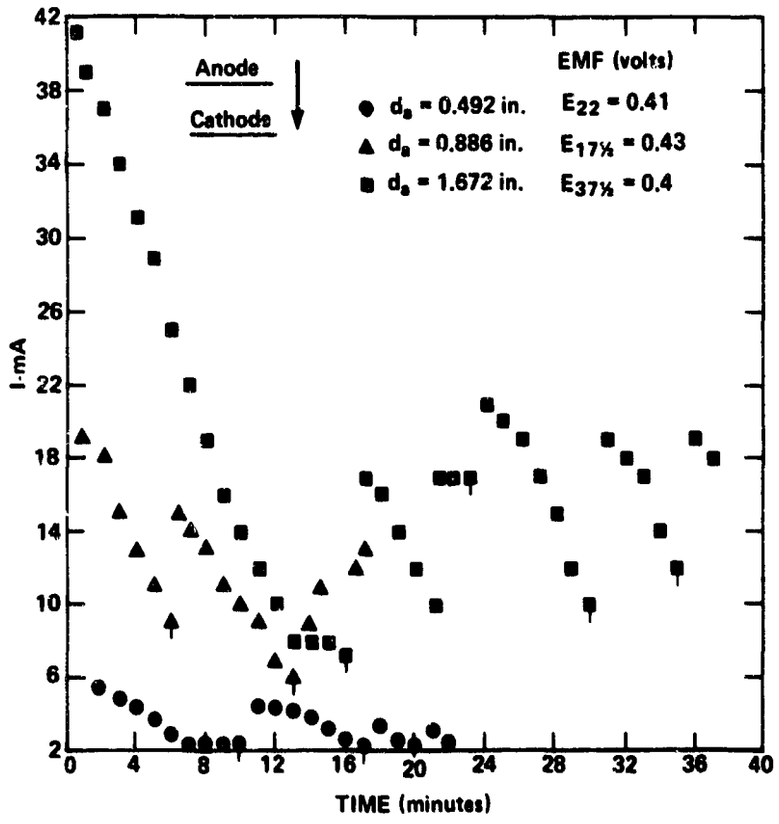

Fig. 16 EFFECT OF NITROGEN INJECTION ON THE CURRENT-TIME CHARACTERISTICS FOR THREE DIFFERENT ANODE AREAS AT A_c/A_a = 1.00 AND ℓ = 0.098 INCH

A true comparison of the data for the d = 0.492-in anode in Figs. 16 and 8 cannot actually be made. This is because of an order of magnitude difference in the steady-state currents at t = 10 min and the first appearance of natural convection at t = 16 min, where I increased from 0.82 mA to only 1.1 mA. However, at t = 20½ min the current increased from 0.30 mA to 1 mA, a 233% increase which is much greater than the percentage increase in Fig. 16 in going from 2 mA to 4 mA. Close inspection of the experimental conditions revealed that the 0.492-in anode in Fig. 8 was etched about ten times in HCl, whereas the anode in Fig. 16 was etched not more than four times. Since it is well known in seawater battery studies that the chemical nature of Mg anodes as well as the level of impurities can alter significantly the performance characteristics (Ref. 13), the above explanation appears to be the primary reason for these discrepancies.

It is interesting to note that the cell EMF was independent of the mode and amount of N_2 injected through the anode. For the runs in Figs. 14, 15, and 16 the EMF only varied between 0.40 - 0.48 volt.

Reactive Gases -- Oxygen and Chlorine

In the preceding section it was seen that the effects of N_2 injection were to depolarize the cell via H_2 removal, thereby leading to an increase in the current. In these former tests the current increase was such that it was generally well below the current at t = 0 min; for the few cases in which it was not, it was only nominally above the value at t = 0 min. The purpose of the present section is to examine the effects of injection of reacting gases -- oxygen and chlorine -- on cell behavior.

In Fig. 17 N_2 and O_2 injections are compared for vertical electrodes, and the effect of O_2 injection on horizontal orientation (cathode lower) is also examined. For the vertical orientation the currents before injection agree to better

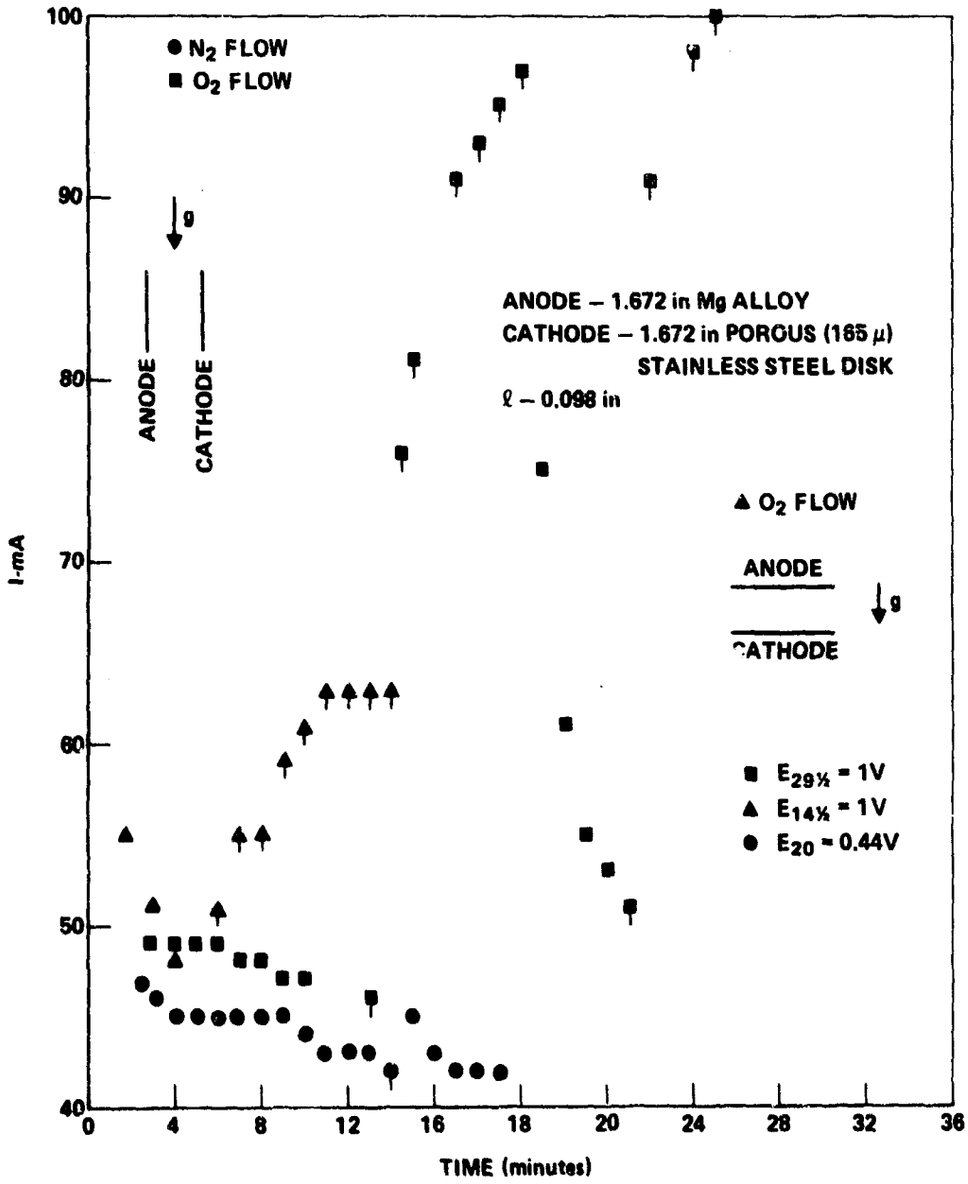

Fig. 17 CURRENT-TIME CHARACTERISTICS FOR NITROGEN VERSUS OXYGEN INJECTION IN TWO CELL ORIENTATIONS; A_c/A_a = 1.00, ℓ = 0.098 IN.

than 10%; however, following N_2 injection at $t = 14$ min I increased from 42 mA to only 45 mA, whereas for O_2 injection I went from 46 mA at $t = 13$ min to 97 mA at $t = 20$ min (note that injection was continuous). At $t = 20$ min the O_2 flow was stopped, and cell polarization then reduced the current over the next 5 min to 51 mA. At $t = 25$ min the O_2 flow was again started and this led to a current of 100 mA at $t = 29$ min. The EMF for the cell at $t = 29\frac{1}{2}$ min was 1 volt, with and in the absence of flow.

For the horizontal orientation, injection of O_2 at $t = 6$ min increased the current from 51 mA to 63 mA. The value of 63 mA is in close agreement with the value one obtains by linear extrapolation of I to $t = 0$. Again the voltage measured was 1 volt (no flow).

In Fig. 18 the effects of O_2 injection in solutions of $C^* = 7$ g/l, 42 g/l, and 112 g/l are examined for vertical orientation for the $d_a = 1.672$-in cell at $A_c/A_a = 1.00$. Note also the data given in Fig. 13 for the $d = 0.492$-in anode, $A_c/A_a = 1.00$. The $C^* = 7$ g/l test has been discussed in the previous figure; it is only included for comparative purposes. For the $C^* = 112$ g/l, two individual curves were obtained; the one with the ▼ symbol was obtained on an old Mg electrode that had undergone a vigorous reaction. The ▲ symbol curve was obtained with a freshly etched Mg electrode. A discrepancy of this magnitude was previously observed with frequently etched electrodes (see the second paragraph of this section). For these curves a moderate ($\sim$ 20%) increase is noted in the current following injection in the continuous or pulse-type modes. However, the baseline current is much higher than that obtained even after injection for the $C^* = 7$ g/l test. The current for the $C^* = 42$ g/l curve following injection was measured incorrectly and thus is not included in the plot. In addition to noting the strong dependence of I versus t on concentration, it is important to again note that the EMF in these tests varied only from 0.87 volt to 1 volt.

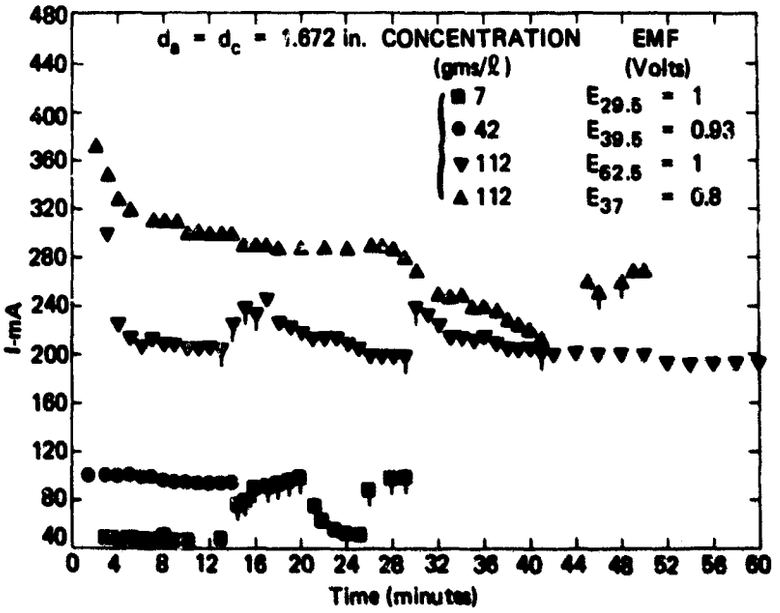

Fig. 18 EFFECT OF OXYGEN INJECTION AND SALINITY ON THE CURRENT-TIME CHARACTERISTICS FOR A VERTICALLY ORIENTED CELL AT A_c/A_a = 1.00, ℓ = 0.098 INCH

In Fig. 19 the current-time behavior for chlorine injection is given for vertical orientation for two cells where d_a = 1.672 in and d_a = 0.492 in, both at A_c/A_a = 1.00. For the d_a = 1.672-in anode the cell was pulsed for approximately 2 sec at t slightly less than 11 min. This led to a rather abrupt increase in the current from 310 mA to 510 mA. At t = 12 min a Cl_2 pulse of about 1 sec again increased the current to 500 mA. A reading was not obtained during the 1-min interval between these pulses. However, when the Cl_2 injection was stopped, at t = 12 min, the current decreased to its baseline value of about 300 mA. Continuous injection of Cl_2 at t = 29 min where I = 210 mA for 1 min led to a dramatic increase in current to 900 mA. The current decreased in 3 min to its steady-state value of 200 mA. The cell EMF (without injection) was equal to 1.25 volts. One should also note that I before injection is equal to the value in Fig. 18 for the ▲ symbol run. Both tests were made with freshly etched anodes.

For the d = 0.492-in anode another dramatic increase in current occurred from I = 29 mA to a maximum of I = 90 mA. The cell EMF at t = 19 min was 0.82 volt (no flow), while at t = 20 it was 1.05 volts. Allowing the cell to remain an additional 13 min without injection of any type a value of 0.47 volt was obtained. Thus it is seen that the effect of addition of small amounts of Cl_2 or oxygen is to increase both the current and the EMF via a chemical reaction. When the reaction goes to completion the behavior typical of the cell without gaseous injection is obtained. For continuous injection over a 10-min interval at C* = 112 g/l the current increased from 1 A to 2.35 A while the EMF was 1.5 volts. This amounts to values of J, P_D, and P_{DV} of J = 154 A/ft^2, P_D = 231 W/ft^2, and 17.3 kW/ft^3. For C* = 25 g/l, i.e., a salinity representative of actual seawater, and a similar chlorine injection period the maximum current was around 2.7 A and the EMF was 1.45 volts. This gives values of J = 177 A/ft^2, P_D = 257 W/ft^2, and P_{DV} = 19.2 kW/ft^3, which are slightly greater than the values for C* = 112 g/l (J = 154 A/ft^2, P_D = 231 W/ft^2, P_{DV} = 17.3 kW/ft^3). This latter test shows that salinity is not an important

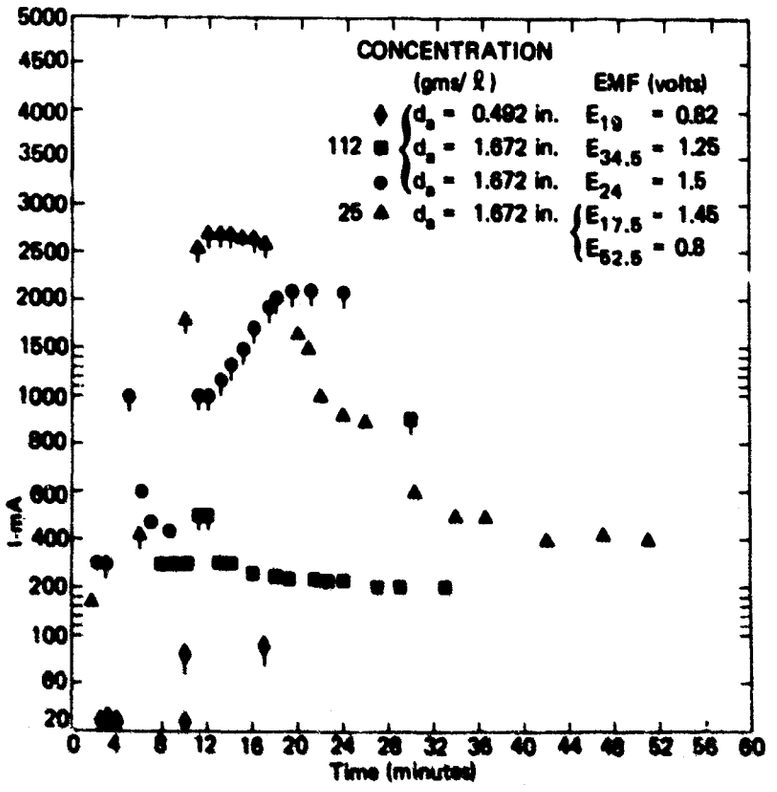

Fig. 19 CURRENT-TIME CHARACTERISTICS FOR CHLORINE INJECTION AND VERTICAL CELL ORIENTATION AT A_c/A_a = 1.00, ℓ = 0.098 INCH

parameter for chlorine injection. Here part of the cathode eroded while a rust colored compound deposited on the anode. The pH's for the solution bulk and for the liquid on the anode were 2 and approximately 4, respectively.

In Fig. 20 the effect of an external resistance on the current-time characteristics is examined. Resistances of R = 200Ω, 1,125Ω, 5,000Ω, and 12 000Ω were connected in line with the anode. An orderly decrease in current with increasing resistance is observed, and, upon removing the load, an abrupt increase in the current takes place. For the 12K resistor, the current increased from 50μA to 125μA following Cl_2 injection. For the 200Ω resistor, at t = 38½ min to t = 44 min, the current varied from 6.7 mA to 6.4 mA, respectively. This is more than 2½ times its value of 2.4 mA at t = 10½ min without Cl_2 injection. At t = 48 min for R = 1125Ω, the injection of Cl_2 led to only a nominal increase in the current from 1.3 mA to 1.6 mA. This is apparently due to electrode deterioration with continuous Cl_2 injection as confirmed by inspection of the electrodes immediately after completion of the test.

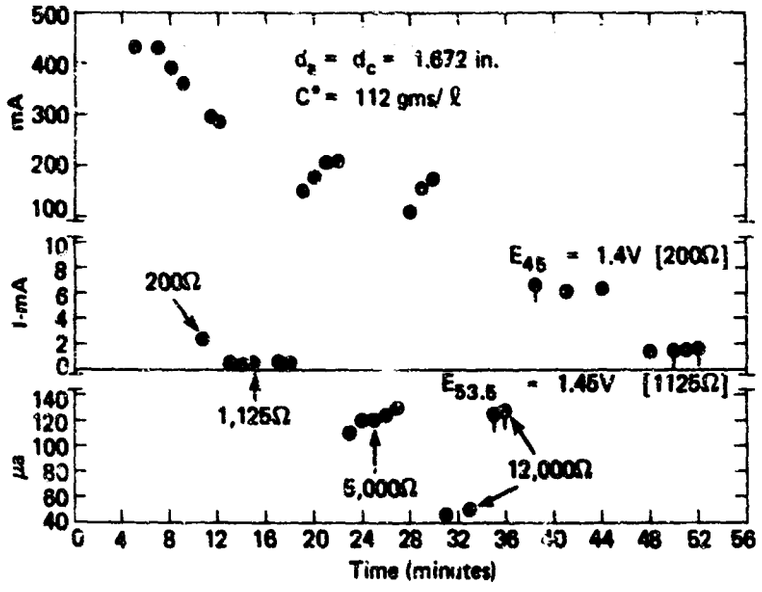

Fig. 20 CURRENT-TIME CHARACTERISTICS FOR CHLORINE INJECTION AT DIFFERENT EXTERNAL RESISTANCES FOR VERTICAL CELL ORIENTATION; $A_c/A_a = 1.00$, $\ell = 0.098$ INCH

4. SUMMARY OF PERTINENT EXPERIMENTAL OBSERVATIONS

NONFLOW

1. Vertically oriented electrodes produce a greater power output than horizontal electrodes. The least favorable performance characteristics were obtained with the anode in the lower position—horizontal orientation.

2. The smallest interelectrode spacing tested, 0.098 in, produced higher overall power outputs than either the 0.315-in or the 0.63-in spacings.

3. The current and power densities were not radially uniform for the orientations tested -- vertical and horizontal (cathode lower).

4. Variations in salinity strongly influenced the current-time characteristics.

5. The EMF for a polarized cell varied between only 0.4 - 0.5 volt and was independent of A_c/A_a, salinity, interelectrode spacing, cell power output, and time. A slight dependence on cathode pore size was observed.

GASEOUS INJECTION

Nonreactive Nitrogen

Nitrogen had to be injected in a pulse-type manner (on-off) in order to increase the baseline current. An increase in the polarized cell current up to about 100% was obtained on the horizontally oriented cell (cathode lower); increases less than 12% were obtained for the vertical and the anode lower arrangements. The cell EMF, varying between 0.40 - 0.48 volt, was independent of the mode and amount of N_2 injected.

Reactive -- Oxygen and Chlorine

Continuous O_2 injection led to a 100% increase in the current over its estimated value at $t = 0$ for the vertical orientation. The increase was salinity-dependent. For the horizontal orientation the overall current increase was modest. The cell EMF following O_2 injection (with or without flow) was around 1 volt.

Dramatic increases in current were obtained for either a pulse- or continuous-type mode of Cl_2 injection for the vertical orientation. For the pulse-type mode the current increased by about 70% over its apparent value at $t = 0$, whereas it went up about 7000% for continuous injection. The cell voltage varied from 0.8 volt to 1.50 volts for a $d = 1.672$-in anode ($A_c/A_a = 1.00$).

5. CELL PERFORMANCE

In this section comparisons are made between cell currents and power densities for a selected number of runs. A calculation of the minimum cell volume required to provide 35 kW of power for Cl_2 injection is also included.

In Tables 1 and 2 are computed values of current density, J (A/ft^2), power density (W/ft^2), P_D, and maximum power density based on cell volume, P_{DV} (W/ft^3), for horizontal and vertical orientations, respectively. The brackets (min) and (mA) indicate the time at which the voltage was measured and the value of current used to compute the current density. Although the actual thicknesses of the Mg anodes were 1/16 in and the porous cathodes 1/8 in, a value of 1/32 in was used in computing P_{DV}. A negligible amount of Mg was used during any run while the cathode is inert and undergoes no erosion. Even if 2 A were drawn for 1 hour, Faraday's law requires that 0.0745 g equivalents of Mg or 0.906 g Mg undergo reaction. For a disk of 1/32-in thickness and diameter d = 1.672 in only 0.0142 in of the Mg would erode ($\rho_{AZ31B\text{-}O_{Mg}}$ = 0.064 lb/in^3). Thus, a 1/32-in thick Mg sample is a very conservative anode thickness.

The current measured covered a very wide range -- from 0.32 mA to 2700 mA, while the voltages ranged between 0.4 volt and 1.50 volts. Current densities and power densities did not exceed 4.8 A/ft^2 and 3.8 W/ft^2, respectively, even with O_2 or N_2 injection when $C^* \leq 7$ g/l. These values are much lower than the maximum values reported in Ref. 10 where J = 18 A/ft^2 and P_D = 8.1 W/ft^2 for the AZ31B-O alloy and a palladium and nickel coated screen (double 8 mesh) cathode. For C^* = 42 g/l and O_2 injection J = 11.4 A/ft^2 while P_D = 9.9 W/ft^2. The highest values of J and P_D for O_2 injection were obtained when C^* = 122 g/l - J = 18.6 A/ft^2 and P_D = 16.8 W/ft^2. Dramatic increases in J and P_D were obtained with the Cl_2 injection. For the d = 1.672-in anode, J = 177 A/ft^2 and P_D = 257 W/ft^2; while, for the d = 0.492-in anode, J = 68.5 A/ft^2 and P_D was as high as 72 W/ft^2.

THE JOHNS HOPKINS UNIVERSITY
APPLIED PHYSICS LABORATORY
SILVER SPRING MARYLAND

Table 1

Performance Characteristics for Horizontal Electrodes (Cathode -- 165μ Stainless Steel)

	Diameter of Anode (in)	Diameter of Cathode (in)	A_c/A_a	Cell Spacing (in)	C* (g/ℓ)	Injection Type	Current Range (mA)	EMF Volts (min)	J^* A/ft^2 (mA)	P_D* (W/ft^2)	P_{DV}** (W/ft^3)
Cathode Lower	0.492	0.492	1.00	0.63	7	--	1.7 - 4.1	0.43 (25½)	1.52 (2)	0.655	10
	0.492	0.492	1.00	0.315	7	--	0.94- 4.7	0.43 (25)	1.14 (1.5)	0.49	16
	1.672	1.672	1.00	0.098	7	N_2 (Pulse)	7 - 42	0.40 (37½)	0.92 (14)	0.37	28
	1.672	1.672	1.00	0.098	7	O_2 (Continuous)	48 - 63	1.00 (14½)	3.8 (58)	3.8	285
Cathode Upper	1.672	0.492	0.0865	0.098	7	--	1.9 - 8.4	0.43 (32)	0.197 (3)	0.0842	6
	0.492	0.492	1.00	0.098	7	N_2 (Pulse)	2.3 - 2.8	0.44 (10)	1.9 (2.5)	0.835	63

*Based on anode area and the cell's steady state or a mean current from the I versus t plots.

**Assumes 1/32 in for the thicknesses of the anodes and cathodes; no allowance is made for the electrode holders.

THE JOHNS HOPKINS UNIVERSITY
APPLIED PHYSICS LABORATORY
SILVER SPRING, MARYLAND

Table 2

Performance Characteristics for Vertical Electrodes (Cathode -- 165μ Stainless Steel, A_c/A_a = 1.00, ℓ = 0.098 in)

Diameter of Anode (in)	Diameter of Cathode (in)	C* (g/ℓ)	Injection Type	Current Range (mA)	EMF Volts (min)	J* A/ft^2 (mA)	P_D* (W/ft^2)	P_{DV}** (W/ft^3)
0.492	0.492	0.035	--	0.32 - 0.40	0.49 (20)	0.267 (0.35)	0.13	10
0.886	0.886	0.35	--	3.8 - 4.1	0.42 (20)	0.915 (3.9)	0.384	29
0.492	0.492	7	--	5.9 - 6.7	0.43 (37½)	4.8 (6.3)	2.06	154
0.492	0.492	7	N_2	4.9 - 5.3	0.40 (15)	3.96 (5.2)	1.59	119
0.492	0.492	42	O_2 (Pulse and Continuous)	10 - 17	0.87 (37½)	11.4 (15)	9.9	740
1.672	1.672	112	O_2 (Continuous)	210 - 370	0.90	18.6 (280)	16.8	1260
1.672	1.672	25	Cl_2	170 -2700	1.45 (17½)	177+ (2700)	257	19 150
0.492	0.492	112	Cl_2	26 - 90	0.82 (19) 1.05 (20)	68.5+ (90)	56 (0.82 Volt) 72 (1.05 Volts)	4200 5380
1.672	1.672	112	Cl_2	300 -2350	1.5	154+ (2350)	231	17 300

*Based on anode area and the cell's steady state or a mean current from the I versus t plots.

**Assumes 1/32 in for the thicknesses of the anodes and cathodes; no allowance is made for the electrode holders.

+Based on the maximum values of I.

For chlorine injection, $P_{DV_{max}}$ was as high as 19.2 kW/ft^3. Thus, the minimum electrode volume needed to produce 35 kW is only 1.83 ft^3. In the Appendix, the amount of chlorine needed to provide 35 kW for 1 hour with $A_c = A_a = 2.4$ ft^2 is 19.9 ft^3. This is too high from our viewpoint. However, the amount of Cl_2 that reacted chemically is believed to be much less than this amount and, therefore, a practical cell could still be developed by recycling any unreacted chlorine from cell to cell.

6. DISCUSSION

SEAWATER REACTION MECHANISM

Explanations are offered for the increased voltages following O_2 and N_2 injection based on the seawater reaction mechanism and application of the Nernst equation.

For a cell operating reversibly, the voltage, E, is given by the Nernst equation:

$$E = E^{o} - \frac{RT}{\varphi F} \ln \frac{(a_{p_1})^{n_1} \times (a_{p_2})^{n_2} \cdots (a_{p_n})^{n_n}}{(a_{r_1})^{m_1} \times (a_{r_2})^{m_2} \cdots (a_{r_m})^{m_m}}, \quad (1)$$

where E^{o} is the difference in the standard half-cell voltages, R is the gas constant, T the absolute temperature, φ the number of equivalents, F the Faraday constant, a_{p_n} the activity coefficient of the n-th product, a_{r_m} the activity coefficient of the r-th reactant, and n_n and m_m are the stoichiometric coefficients. For pure Mg the difference in the half-cell voltages for the seawater battery is $E^{o} = 1.542$ volts. For the AZ31B-O Mg alloy an estimated value of E^{o} is 1.48 volts (see Appendix).

For the cell reaction scheme

Anode

$$Mg \rightarrow Mg^{++} + 2e$$

$$\frac{2}{3} Al \rightarrow \frac{2}{3} Al^{+++} + 2e$$

$$Mn \rightarrow Mn^{++} + 2e$$

$$Zn \rightarrow Zn^{++} + 2e$$

Cathode $\quad 8H_2O + 8e^- \rightarrow 8OH^- + 4H_2$

we obtain

$$Mg + \tfrac{2}{3}\,Al + Mn + Zn + 8H_2O \rightarrow Mg(OH)_2 + \tfrac{2}{3}\,Al(OH)_3 + Mn(OH)_2 + Zn(OH)_2 + 4H_2$$

for the overall cell reaction. The Nernst equation becomes

$$E_{298} = 1.48 - \frac{0.0592}{2} \log \frac{a_{Mg(OH)_2}\, a_{Al(OH)_3}^{2/3}\, a_{Mn(OH)_2}\, a_{Zn(OH)_2}\, a_{H_2}^{4}}{a_{Mg}\, a_{Al}^{2/3}\, a_{Mn}\, a_{Zn}\, a_{H_2O}^{8}}, \qquad (2)$$

where the number of equivalents transferred per metal is 2. For a cell voltage of $E = 0.45$ volt, which corresponds to the mean of the measured polarized cell voltages (for no flow and nitrogen injection), the Nernst equation requires that

$$\frac{a_{Mg(OH)_2} \cdots\cdots a_{H_2}^{4}}{a_{Mg} \cdots\cdots\cdots a_{H_2O}^{8}} = 10^{35} .$$

Since the activity coefficient is proportional to concentration a value for the above ratio close to the order of 10^{35} follows from the solubility product constants for the metallic hydroxides which are (Ref. 14):

$$Mg(OH)_2 \rightleftharpoons Mg^{++} + 2OH^- \qquad K_{sp} = 10^{-11}$$

$$Mn(OH)_2 \rightleftharpoons Mn^{++} + 2OH^- \qquad K_{sp} = 10^{-13}$$

$$Zn(OH)_2 \rightleftharpoons Zn^{++} + 2OH^- \qquad K_{sp} = 10^{-17}$$

$$Al(OH)_4 \rightleftharpoons Al(OH)_3 + OH^- \qquad K_{sp} = 2.5 \times 10^{-2}$$

Aluminum can also precipitate out as the oxide Al_2O_3. Because aluminum is amphoteric, both strongly basic and acidic solutions will increase its solubility in solution. Its K_{sp} value is subject to discussion since pH's of 8.5 were obtained at high reactivity. Incorporating the activities of the metals Mg, Al, Mn, and Zn, which are given by their respective mean weight fractions, 0.958, 0.03, 0.002, and 0.01, (see Appendix) into the ratio of the products of the activities gives

$$\frac{a_{Mg(OH)_2}^{\cdots\cdot 4} \cdot a_{H_2}}{a_{Mg}^{\cdots\cdots 8} \cdot a_{H_2}} \simeq 10^{35}\, a_{H_2}^{\;4} \; .$$

Here a_{H_2O} was set equal to $a_{H_2O} = 1.00$ in accordance with standard electrochemical conventions. The activity of H_2 remains an unknown; however, if a_{H_2} does not deviate too far from unity, then E_{298} would be equal to $E_{298} \simeq 0.45$. Without actually measuring the partial pressure of H_2 one cannot determine a_{H_2}. For present purposes we are setting $a_{H_2} = 1.00$ as required by the Nernst equation. There are additional reactions such as the secondary reaction,

$$2NaOH + MgCl_2 \rightarrow 2NaCl + Mg(OH)_2 \; ,$$

and the solution reactions,

$$CaSO_4 \rightleftharpoons Ca^{++} + SO_4^{=} \qquad K_{sp} = 1.95 \times 10^{-4}$$

$$Ca^{++} + CO_3^{=} \rightleftharpoons CaCO_3 \downarrow \qquad K_{sp} = 10^{8}$$

$$Mg^{++} + CO_3^{=} \rightleftharpoons MgCO_3 \downarrow \qquad K_{sp} = 3.85 \times 10^{4}$$

where $CO_3^{=}$ results from the solubility of ambient CO_2 in H_2O, which are of lesser importance and, thus, should not greatly affect the overall cell reaction in Eq. (2).

The addition of O_2 and Cl_2 through the porous cathode led to increases of the polarized cell voltage from the 0.4 - 0.5-volt range up to a range from around 1 volt to 1.50 volts. Taking $E_{298} = 1.00$ and assuming that the overall cell reaction is still given by Eq. (2), i.e., at least for O_2 injection, we obtain a value of order 10^{16} for the ratio of the products of the activity coefficients. This would require that the concentration of one or both products be lowered and/or the activity of the reactants be increased. Changes in the activities of the reactants leading to an order of magnitude change of 10^{19} are unlikely; the volume of H_2O was actually observed to decrease slighily during a vigorous cell reaction, and a decrease in a_{Mg} would be offset by further dissolution of the Mg electrode. A direct reaction of O_2 with H_2 to form H_2O on the stainless steel cathode, thereby reducing a_{H_2}, is unlikely because a two-body recombination reaction of gases must occur either on the stainless steel cathode (a noncatalyst) or in solution. Also, O_2 does not alter the solubility of the insoluble metal hydroxides. One remaining reaction scheme is for an additional electrochemical reaction to occur at the cathode, thereby raising the E^o value while maintaining the primary reaction in Eq. (2). From the standard oxidation-reduction charts (e.g., Ref. 15) we obtain

	E^o
$O_2 + 2H_2O + 4e^- \rightarrow 4OH^-$	0.40
$4H_2O + 4e^- \rightarrow 4OH^- + 2H_2$	-0.828
Overall Cathode Reaction $O_2 + 6H_2O + 8e^- \rightarrow 8OH^- + 2H_2$	-0.428 volt.

Thus, the overall cell reaction is

Anode	$\sum_{i=1}^{3} M_i + \frac{2}{3} Al \rightarrow \sum_{i=1}^{3} M_i^{++} + \frac{2}{3} Al^{+++} + 8e^-$	2.30 V
Cathode	$O_2 + 6H_2O + 8e^- \rightarrow 8OH^- + 2H_2$	-0.428 V
Overall Cell Reaction	$\sum M_i + \frac{2}{3} Al + O_2 + 6H_2O \rightarrow \sum M^{++} + \frac{2}{3} Al^{+++} + 8OH^- + 2H_2\uparrow$	1.882 volts

Here M_i and M_i^{++} are used to denote the metals Mg, Zn, Mn, and their ions, respectively. The Nernst equation for this two-step cathode reaction is

$$E_{298} = 1.882 - \frac{0.0592}{2} \log \left(\frac{a_{Mg(OH)_2} \, a_{Al(OH)_3}^{2} \, a_{Mn(OH)_2}^{3} \, a_{Zn(OH)_2} \, a_{H_2}^{4}}{a_{Mg} \, a_{Al}^{2} \, a_{Mn}^{3} \, a_{Zn} \, a_{H_2O}^{8} \, a_{O_2}} \right). \quad (3)$$

with the exception of a_{O_2} in the denominator of the ratio of activity coefficients and the E^o value equal to $E^o = 1.882$, identical to Eq. (2). For a value of 10^{35} for the ratio of activity coefficients $E_{298} = 0.85$, while for 10^{30} we obtain $E_{298} = 1.00$. This covers the range of the measured cell EMF's.

For Cl_2 injection a direct reaction to the chlorides is conceivable. This would lead to a reduction of the activity coefficients of the metal hydroxides and a corresponding increase in the cell EMF. A number of electrochemical reaction schemes are possible for Cl_2 injection; one that gives a reasonable net value for E^o and also allows for soluble metal chloride formation is

		E^o
	$4Cl_2 + 8e^- \rightarrow 8Cl^-$	1.360
Cathode	$8H_2O + 8e^- \rightarrow 8OH^- + 4H_2\uparrow$	$\frac{-0.828}{0.532}$ volts
Anode	$\sum_{i=1}^{3} M_i + \frac{2}{3} Al \rightarrow \sum_{i=1}^{3} M_i^{++} + \frac{2}{3} Al^{+++} + 8e^-$	2.31
	$4Cl^- + 8OH^- \rightarrow 4ClO^- + 4H_2O + 8e^-$	$\frac{-0.94}{1.37}$ volts

Overall Cell Reaction

$$4Cl_2 + 4H_2O + \sum_{i=1}^{3} M_i + \frac{2}{3} Al \rightarrow \sum_{i=1}^{3} M_i^{++} + \frac{2}{3} Al^{+++} + 4H_2 + 4Cl^- + 4ClO^- \quad 1.90 \text{ volts}. \quad (4)$$

Since the products of this reaction are soluble salts, the ratios of the activity coefficients cannot approach values of the order of 10^{35} for $E_{298} \sim 1$ volt. It appears likely therefore, that the primary cell reaction in Eq. (2) also occurs at reduced values for the activity coefficients of the metallic hydroxides. That is, the injection of Cl_2 gas leads to a partial dissolution of the insoluble hydroxides at a reduced value of E_{298}. The overall cell reaction, thus the cell EMF, is therefore a combination of the primary seawater reaction (Eq. (2)) and the complex reaction scheme (Eq. (4)).

CHARGE TRANSPORT

A fundamental approach to an understanding of the complex transport processes occurring in a seawater battery would require a solution to the multicomponent equations of continuity, motion, and charge transport subject to appropriate boundary conditions at the anode and cathode. Such a study would be of great value because the scale-up of a small laboratory-size battery to a practical prototype could be readily accomplished. Since this would require a great effort and is also not warranted at this time because the reaction mechanisms at the anode and cathode are not sufficiently well understood, a semiquantitative approach is adopted in order to outline possible alternative approaches.

If we assume the solution can be represented by a single component, uni-univalent electrolyte, then a solution to the time-dependent transport equation for charge (Ref. 16)

$$\frac{\partial q}{\partial t} = D\nabla^2 q - q/\tau - \vec{v}\cdot\nabla q + D'F\nabla^2 C - \frac{D(\nabla C)^2}{q/F} \qquad (5)$$

where

$$q = F(C_+ - C_-) \qquad D' = D_+ - D_-/2 \qquad C = C_+ + C_-$$

$$D = D_+ + D_-/2 \qquad \tau = \varepsilon\varepsilon_0/K$$

and integration over the electrode area would provide the current density-voltage versus time characteristics. Other standard definitions are for the conductivity, K, and the ionic mobility u:

$$K = u\,C\,F \tag{6}$$

$$u = \frac{D\,F}{R\,T} \quad . \tag{7}$$

The terms in Eq. (5) from left to right are the diffusive, conductive, convective, and nonlinear fluxes, respectively. An order of magnitude comparison is made for these terms below.

The primary ions undergoing reaction in the seawater battery are Mg^{++}, OH^-, H_3O^+, Na^+, and Cl^-. The ionic mobilities for H_3O^+ and OH^- are 3.64×10^{-3} cm^2/volt-sec and 2.05×10^{-3} cm^2/volt-sec, respectively, while the mobilities for Mg^{++}, Na^+, and Cl^- are all about 5×10^{-4} cm^2/volt-sec. The remaining ions $SO_4^=$, K^+, Ca^{++} from the compounds Na_2SO_4, KCl, and $CaSO_4$ are also in the above range of values. Thus a reasonable mean value of u is $u = 1 \times 10^{-3}$ cm^2/volt-sec. Most ionic diffusion coefficients are about 10^{-5} cm^2/sec. For the highest salt concentration $C^* = 112$ g/l the total concentration of equivalents in solution is 2×10^{-3} eq/cc. The conductivity from Eq. (6) is then $K \simeq 0.2\ \Omega^{-1}cm^{-1}$. A reference value for q is $q = FC = (96\,500)(2\times10^{-3}) = 1.9 \times 10^{-2}$ C/cc. Now from Eq. (5) we obtain

$$D\nabla^2 q \simeq Dq/L^2 \simeq \frac{(10^{-5})(1.9\times10^{2})}{(2.5\times10^{-1})^2} \simeq 0(10^{-1})$$

$$q/\tau = \frac{K}{\varepsilon\varepsilon_0}\,q \simeq \frac{(2\times10^{-1})(1.9\times10^{2})}{(80)(8.85\times10^{-14})} \simeq 0(10^{12})$$

$$v \cdot \nabla q \simeq v\,q/L = 0 \quad \text{(No Flow)}$$

$$D'F\nabla^2 C \simeq D'FC/L^2 \quad \frac{(5\times10^{-6})(9.65\times10^{4})(2\times10^{-3})}{(2.5\times10^{-1})^2} \simeq 0(10^{-1})$$

$$D(\nabla C)^2/q|F \simeq D\ C/L^4 \simeq \frac{(10^{-5})(2\times10^{-3})}{(2.5\times10^{-1})^4} \simeq 0(10^{-5}) \ .$$

The overwhelmingly large value for q/τ clearly indicates that ohmic conduction is the dominant factor. Now the flux of charge at the electrode surface is given by

$$J = -D\nabla q - D\ F\nabla C - K\nabla\psi + \vec{v}q + j_a + j_c \qquad (8)$$

where j_a and j_c refer to the fluxes due to the rate of dissolution of the Mg anode, and J_c refers to the net difference between the rate of formation and rate of removal of H_2. An order of magnitude estimate for these electrode fluxes is:

$$D\nabla q \simeq \frac{(10^{-5})(1.9\times10^{2})}{(2.5\times10^{-1})} \simeq 0(10^{-2})$$

$$D'F\nabla C \simeq D'F\ C/L \quad \frac{(5\times10^{-6})(9.65\times10^{4})(2\times10^{-3})}{(2.5\times10^{-1})} \simeq 0(10^{-2})$$

$$K\nabla\psi \simeq K\ \psi/L \simeq \frac{(0.2)(0.45)}{(2.5\times10^{-1})} \simeq 0(10^{-1})$$

$$vq \simeq v_{o1}q \simeq \frac{6\times10.5}{100}\ (1.9\times10^{2}) \simeq 0(10^{2})$$

j_a, j_c — Uncertain .

Here the liquid flow velocity, v_{ol}, (arbitrarily taken as 1/100 of the superficial gas velocity) times q term dominates. In the absence of flow the conductive term dominates. However, the j_a and j_c fluxes appear to be equally important as shown by the experimental I versus t plots.

It is interesting to examine the boundary condition for steady state conditions. Here $j = 0$, and since diffusive transport is slower than conductive transport, Eq. (8) becomes for one-dimensional geometry

$$D\nabla q \simeq \frac{KRT}{2\eta_+ F\lambda} (1 - C_s/C_o) = j_a + j_c \ , \qquad (9)$$

where

$$\lambda = d/Nu \qquad (10)$$

$$Nu = hd/D \qquad (11)$$

and C_s and C_c refer to concentrations at the surface and solution bulk, respectively. Here λ is the so-called film thickness, d is a reference length, Nu is the Nusselt number, and h is a charge transfer coefficient. It appears possible that one can employ a procedure similar to that in Ref. 17 in order to deduce the h dependence on experimental parameters. Presently this is not possible because of lack of a nondimensional correlation for the experimental data and a solution to the charge transport equation.

A well-accepted approach that may be used to correlate the experimental data for the purpose of scaling up to a larger cell is dimensional analysis. Two major drawbacks in the use of this type of procedure are:

1. It assumes a simple product of powers dependence for the dependent variable. In many cases exact solutions do not reduce to simple formulas over wide ranges of experimental conditions.

2. It does not give us a mechanistic interpretation of the reaction or reactions, which would provide a valuable input in the design of a battery for optimum performance.

Nevertheless, it is a powerful tool because, if the variables are properly selected, the number of experiments can be reduced by orders of magnitude through variations in only the resulting nondimensional groups.

The polarized cell current, I_{ss}, was observed to depend upon the following: A_a, A_c, ℓ, $\dot{M}_a - \chi \dot{M}_c$, and FC^o where ℓ is the interelectrode spacing, $\dot{M}a$ the rate of dissolution of the anode, χ a hydrogen blocking factor, $\dot{M}_c$ a removal rate of hydrogen, and FC^o the initial concentration of salt expressed in C/eq, a measure of the salinity. Other parameters which are important are the fluid viscosity, μ, density, ρ, and diffusion coefficient, D. Following the procedure outlined in Ref. 18 we obtain the following matrix in the MLTQ (mass, length, time, charge) system.

	k_1	k_2	k_3	k_4	k_5	k_6	k_7	k_8	k_9
	I_{ss}	A_a	A_c	ℓ	μ	ρ	D	$\dot{M}_a - \chi \dot{M}_c$	FC^o
M	0	0	0	0	1	1	0	1	0
L	0	2	2	1	-1	-3	2	0	-3
T	-1	0	0	0	-1	0	-1	-1	0
Q	1	0	0	0	0	0	0	0	1

The rank of the right-hand matrix is nonzero; therefore the number of nondimensional products is 9-4 = 5. We obtain the following nondimensional products:

$$\pi_1 = \frac{I_{ss}/FC^o}{\dot{M}_a - \chi\dot{M}_c/\rho} \qquad \pi_4 = \ell/L$$

$$\pi_2 = A_a^{1/2}/L \qquad \pi_5 = v/D = Sc$$

$$\pi_3 = A_c^{1/2}/L$$

where $\dot{M}_a - \chi\dot{M}_c/\rho D$ is a characteristic length, L

$$L = \frac{\dot{M}_a - \chi\dot{M}_c}{\rho D}$$

and Sc is the Schmidt Number for mass transfer. From Buckingham's theorem we obtain

$$I_{ss} = \varphi\left(\frac{(\dot{M}_a - \chi\dot{M}_c)FC^o}{\rho}\right)\left(\frac{A_a}{A_c}\right)^f (\ell/L)^g \, Sc^d \, . \qquad (12)$$

Since $\dot{M}_a \times t$ for the present study is much less than $C_{Mg^{++}}$ in the salt solution, $\dot{M}_a$ could not be determined. For example, if we assume a current of 100 mA for 1 hour, then from Faraday's law we obtain

$$\text{No. of Equivalents of Mg} = \frac{(100 \times 10^{-3})(3600)}{96\,500} = 3.73 \times 10^{-3} \text{ eq}$$

or 0.0453 g. This is much less than the value of 0.78 g given in the Appendix for the solution $C^* = 112$ g/l. In future studies, however, $MgCl_2$ could be omitted from the artificial seawater in order to determine $\dot{M}_a$. No deleterious side effects would be expected in doing so; actually, the rate of diffusion of Mg into solution would be enhanced. It is also noted (Ref. 13) that common anion electrolytes such as $MgBr_2$, thus also $MgCl_2$, cause the anode potential to fall rapidly

with increasing pH, while with NaBr, the anode potential was essentially constant over pH 9.3 to 10.0. For a vigorous reaction, M_c can be determined by measuring the rate of evolution of H_2 on a gas burrette. More sensitive techniques, e.g., use of gas chromatography, would be needed at low H_2 concentrations. The blockage factor χ would be the only difficult parameter to determine since H_2 bubble size, rate of formation, and removal would have to be determined as a function of interelectrode spacing and A_c/A_a. This would have to be accomplished photographically, and interpretation of the data at small interelectrode spacings would be a difficult task.

The intent of the discussions under the Charge Transport section was to outline approaches that may be used to obtain an understanding of the transport mechanisms occurring in a seawater battery. It was also emphasized that such an approach is necessary in order to design a battery for optimum performance. The difficulties involved in a program of this type are also outlined. Here the objective is to draw attention to the need for a long-range study program pursuing a number of the ideas presented herein in conjunction with the experimental effort.

7. CONCLUDING REMARKS

There are a number of important conclusions that can be formed from the present experiments. The one of greatest importance, since it pertains to the overall program, is that the development of a high energy density battery subject to the following rigid constraints,

a. Generate 35 kW of continuous power for periods of around 1 hour,

b. Operate within a cylindrical configuration - 21 inches x 7 feet, i.e., 16.8 ft^3,

c. Be reliable and have good storage properties, and

d. Be cost effective,

appears feasible. A long range study program is therefore recommended.

The initial phase of this study program could proceed along the lines outlined in the detailed study program in Ref. 19. A few of the more important studies that are needed before scale-up to a practical prototype are

a. Performance characteristics for porous magnesium and lithium composites,

An exact determination of the minimum amount of chlorine needed to sustain optimum battery performance,

c. An investigation of recycling unreacted gases from cell to cell in a small lab-size battery,

d. An exploratory study of other less toxic reacting gases and gas mixtures, and

e. A complementary analytical effort.

APPENDIX

ESTIMATION OF MASS FLOW RATES

A porous material may be defined as a solid that contains a large number of holes or pores that may be interconnected or distributed randomly or uniformly throughout the solid. The sintered porous stainless steel cathodes are characterized by highly tortuous and interconnected pore paths. In a previous study on controlled gaseous injection in reentry wakes (Ref. 20) it was shown that there are conditions under which these types of porous materials can provide radially uniform injection velocities. In the context of battery development it is of paramount importance to provide a uniform injection velocity because this will have a direct bearing on the electrochemical reaction (a uniform reaction rate across the electrode surface is desirable).

In Ref. 20 the requirement for a radially uniform injection velocity for a porous material exhibiting overall cylindrical geometry was that $R/\sqrt{K_D} > 10$. Here R is the radius of the porous material and K_D is the permeability, a measure of the ease of flow through a porous medium. The permeability, K_D, is a constant in Darcy's law, which is given by

$$v_o = \frac{K_D}{\mu} \frac{\Delta p}{L} ,$$

where v_o is the superficial velocity, defined as

$$v_o = v/P.$$

Here v is a cross-sectional velocity, and P is the porosity given by

$$\%P = V_p/V_t \times 100\% ,$$

where V_p is the pore volume and V_t is the total volume (solid plus voids). The remaining quantities are μ, the fluid viscosity, Δp, the applied pressure drop, and L, the thickness of the porous material. If the permeability of a material is known, then use of Darcy's law and continuity,

$$\dot{m} = \rho v_o A_{eff} ,$$

where A_{eff} is the cross-sectional area available for flow, allows one to determine $\dot{m}$, the mass flow rate.

The porosities of the stainless steel samples were determined experimentally using the bulk density technique (Ref. 21). Values of 60.5%, 46.5%, and 43% were obtained for the 165μ, 35μ, and the 5μ samples, respectively. These values are close to the value for cubic packing of spheres, which is 47.6%. For cubic packing the void diameter is 0.82 times the grain diameter (Ref. 22). In Table 3 values of permeability are calculated based on geometrical properties (porosity and effective pore diameter) alone. The very low values of K make $R/\sqrt{K} >> 10$ and, therefore, one can expect a radially uniform injection velocity with these stainless steel samples.

In order to calculate v_o from Darcy's law, one needs to know the pressure in the electrode holder. Because a minimum of about 2 feet of tygon tubing separated a bourdon pressure gauge from the plenum chamber, $\dot{m}$ was determined by an alternate procedure. The volume of N_2 injected for similar experimental conditions was measured by displacement of water from an inverted graduated cylinder for different time intervals. The average of seven tests for the volumetric flow rate was 6.6 cc/sec. Now, assuming the same volumetric flow rate for chlorine and standard conditions, we obtain

$$\dot{m} = 6.6 \frac{cc}{sec} \times \frac{70.9 \text{ g } Cl_2}{22\,400 \text{ cc}} \times \frac{1 \text{ lb}}{453 \text{ g}} = 4.6 \times 10^{-5} \text{ lb/sec}$$

Table 3

Permeability Based on Geometrical Properties

Model	Permeability Equation	Permeability for Stainless Steel Samples
Serial	$K_D = \frac{1}{96} Pd^2$	135μ - 1.24×10^{-9} ft^2 29μ - 9.03×10^{-9} 4μ - 7.68×10^{-13}
Kozeny Equation*	$K_D = c/16\ Pd^2$	135μ - 3.70×10^{-9} 29μ - 1.31×10^{-10} 4μ - 2.30×10^{-12}
Ideal Medium	$K_D = (1/32)Pd^2$	135μ - 3.70×10^{-9} 29μ - 1.31×10^{-10} 4μ - 2.30×10^{-12}
Brinkman Drag Theory	$K_D = \frac{d^2}{72}\left\{3 + \frac{4}{1-p} - 3\sqrt{\frac{8}{1-p} - 3}\right\}$	135μ - 1.69×10^{-9} 29μ - 1.88×10^{-11} 4μ - 1.07×10^{-13}

*Kozeny constant taken equal to 0.5, its value for a circle.

Here the pore diameters are the respective void diameters.

If we use the entire cross-sectional area of the cylindrical configuration ($A = 2.4\ ft^2$) for an electrode, then over a 1-hour time period

$$\dot{m}_2 \times t = \dot{m}_1 \frac{A_2}{A_1} t = \frac{(4.6 \times 10^{-5})(2.4)(3600)}{\pi/4\ (1.672 \times \frac{1}{12})^2} = 26\ lb\ Cl_2 .$$

Based on the density of liquid Cl_2 at 20°C of 85 lb/ft^3, the volume occupied is only 0.3 ft^3. However, 63 cells are needed to provide 35 kW. If each cell requires 0.3 ft^3 of Cl_2, then 19.9 ft^3 of Cl_2 would be needed for the 35 kW battery.

Additional tests were carried out to determine the amount of unreacted Cl_2, or the amount of Cl_2 available for recycling from cell to cell in a battery. The results of two successive tests indicated that around a factor of two was available for recycle. This was obtained by passing Cl_2 through the seawater cell with and without the Mg anode in its electrode holder and recording the time required to fill an evacuated chamber from 30 psig (vacuum) to atmospheric. The chamber filled about twice as fast without the Mg anode. Thus, a more realistic value for the 35 kW battery would be around 10 ft^3 instead of the above 19.9 ft^3. It is believed that the minimum amount of Cl_2 needed for efficient cell reaction is somewhat less than $\dot{m} = 4.6 \times 10^{-5}$ lb/sec. This decrease is expected to offset an increase in Cl_2 required for operating below the ideal 100% recycle efficiency. More precise tests using choked orifices would be needed to determine these quantities.

ESTIMATION OF E^o FOR AZ31B-O MAGNESIUM ALLOY

Standard materials handbooks give the following weight percentages for the AZ31B-O magnesium alloy:

Al 2.5 - 3.5%

Zn 0.7 - 1.3%

Mn ~ 0.2% .

Assuming that the E^o's add as $\sum_i X_i E^o_i$ where X_i is the mean weight fraction of the respective metals and E^o_i is the difference between the standard anode $E_{o\,i}$'s and the E_o for the cathode reaction,

$$2\ H_2O + 2e^- \rightarrow 2OH^- + H_2 - 0.828\ V\ ,$$

we obtain the following value for the weighted summation of $X_i\ E_i^o$:

	E_{oi} (volts)	E_i^o	X_i	$X_i\ E_i^o$
$Al \rightarrow Al^{+++} + 3e^-$	1.66	0.832	3%	0.0025
$Mn \rightarrow Mn^{++} + 2e^-$	1.18	0.352	0.2%	0.0007
$Zn \rightarrow Zn^{++} + 2e^-$	0.763	-0.065	1.0%	-0.00065
$Mg \rightarrow Mg^{++} + 2e^-$	2.37	1.542	95.8%	1.477
				$\sum_i X_i E_i^o$ = 1.48 volts

This is not much different from the 1.542 volts for the E^o obtained with pure Mg. However differences will arise in the current because of the greater ease of reaction for pure Mg, e.g., pure Mg will react in air whereas the AZ31B-O Mg alloy requires a strong salt solution to undergo appreciable reaction.

THE JOHNS HOPKINS UNIVERSITY
APPLIED PHYSICS LABORATORY
SILVER SPRING MARYLAND

NUMBER OF EQUIVALENTS IN SOLUTION FOR C* = 112 g/ℓ

1. $NaCl = 85.57\ g\ 10^3 cc \times \frac{1\ eq}{58.45\ g} = 1.47 \times 10^{-3}$ eq/cc

$Na_2SO_4 = 8.67\ g\ 10^3 cc \cdot \frac{2\ eq}{142.05\ g} = 1.22 \times 10^{-4}$

$MgCl_2 = 17.45\ g\ 10^3 cc \times \frac{2\ eq}{95.23\ g} = 3.66 \times 10^{-4}$

$K\,Cl = 2.65\ g\ 10^3 cc \times \frac{1\ eq}{74.56\ g} = 3.55 \times 10^{-5}$

$CaSO_4 = 4.73\ g\ 10^3 cc \times \frac{2\ eq}{136.15\ g} = 9.47 \times 10^{-5}$

Total No. Equivalents 2.1×10^{-3} eq/cc

2. Number of grams of Mg present in the reaction cell:

$$\text{grams of Mg} = \frac{17.45\ g\ MgCl_2}{10^3 cc} \times 175\ cc \times \frac{24.32\ g\ Mg}{95.23\ g\ MgCl_2} = 0.78\ g\ Mg$$

REFERENCES

1. "Problems in Power for Propulsion Applying to Submarines," Prepared by Panel for Propulsion of the National Research Council, Committee on Undersea Warfare, Serial No. NRC: CUW: 0075, Washington, D.C., September 1950.

2. R.C. Hamilton, The Stirling Engine Versus Other Torpedo Propulsion Power Systems, RP-P 484, Vol. 1, IDA 69-9735, Institute for Defense Analyses, Arlington, Va.. April 1969.

3. N.C. Dey, Heat Engines and Applied Thermodynamics, Asia Publishing House, N. Y., 1964, p. 86.

4. C.L. Opitz, "Seawater Power Supply Using a Magnesium-Steel Cell," 4th Intersociety Energy Conversion Engineering Conference, September 1969, pp. 699-704.

5. J.P. Wagner, "Seawater Batteries," APL/JHU BFM-173, 28 January 1970.

6. A.P. Saunders and H. Wroblowa, "High Performance Iodine Cathode," N 69-34813, Institute for Direct Energy Conversion, U. of Penn., Towne School of Engineering, December 1968.

7. H.A. Liebhafsky and E.J. Cairns, Fuel Cells and Fuel Batteries, John Wiley and Sons, Inc., 1968, pp. 524-554.

8. H. Shimotake and E.J. Cairns, "A Lithium/Tin Cell with an Immobilized Fused-Salt Electrolyte: Cell Performance and Thermal Regeneration Analysis," IECEC, 1968, pp. 76-91.

9. F.L. LaQue and G.L. Cox, "Some Observations of the Potentials of Metals and Alloys in Seawater," Proceedings of the Forty-Third Annual Meeting, American Society for Testing Materials, Vol. 40, June 24-28, 1940.

10. B.J. Wilson, Characteristics of an Inert Cathode/Magnesium Anode Seawater Battery, NRL 6715, Naval Research Laboratory, Washington, D.C., June 1968.

11. J.L. Robinson and P.F. King, "Electrochemical Behavior of the Magnesium Anode," J. Electrochem. Soc., Vol. 108, No. 1, January 1961, pp. 36-41.

12. L. Whitby, "The Dissolution of Magnesium in Aqueous Salt Solutions," Trans. Faraday Soc., Vol. 31, 1935, p. 638.

13. R. Glicksman, "Anodic Dissolution of Magnesium Alloys in Aqueous Salt Solutions," J. Electrochem. Soc., February 1959, pp. 83-88.

14. C.W. Pierce, D.T. Sawyer, and E.L. Haenisch, Quantitative Analysis, J. Wiley and Sons, Inc., N. Y., 1958, pp. 457-460.

15. C.L. Mantell, "Electro-Organic Chemical Processing," Chemical Process Review No. 14, Copyright 1968 by C.L. Mantell, Library of Congress Catalog No. 68-21097.

16. J. Gavis, "Non-Linear Charge Transport Equation," Chem. Engng. Science, Vol. 22, 1967, p. 359.

17. J.P. Wagner, Charge Generation During Flow of a Hydrocarbon Liquid Through Micro-Porous Media, PhD. Thesis, Department of Chemical Engineering, Johns Hopkins University, September 1966, pp. 64-67.

18. H.L. Langhaar, Dimensional Analysis and Theory of Models, John Wiley and Sons, N.Y., 1951, pp. 129-142.

19. J.P. Wagner, "Proposal for Detailed Experimental Study on Batteries for Underwater Applications," APL/JHU BFM-215, 20 April 1970.

20. J.P. Wagner and J.M. Cameron, "Controlled Gaseous Injection in Reentry Wakes," Section VII/1b, Research and Development Programs Quarterly Report, October-December 1968, APL/JHU U-PQR/68-4.

21. R.E. Collins, Flow of Fluids through Porous Materials, Rheinhold Publishing Co., N.Y., 1961, p. 8.

22. A.V. Luikov, Heat and Mass Transfer in Capillary-Porous Bodies, Pergamon Press, 1966, p. 212.

ACKNOWLEDGMENT

The author wishes to acknowledge the support and comments given to him by Dr. F. K. Hill and Dr. W. H. Avery during the course of this work. He is also indebted to Mrs. Nancy A. Dollens for typing the rough draft.